Reuse of Food Processing Wastewater in Washington State

Iftaykhairul Alam, Lynne Carpenter-Boggs and Indranil Chowdhury
Department of Civil & Environmental Engineering,
Washington State University,
Pullman, WA 99164, USA

EXECUTIVE SUMMARY

The objective of this study is to investigate the technical feasibility of treating food-processing wastewater to direct potable reuse in Washington State. The agriculture and food-manufacturing sector is a cornerstone of Washington's economy in both rural communities and metropolitan areas. Communities use in excess of 60 percent of their annual potable water to supply food-processing industries. The food processing industries in the arid climate of central Washington are facing challenges due to climate change, water shortage and groundwater depletion. Hence, there is a critical need for reuse of wastewater for sustainability of food processing industries in Washington State. Food processing wastewater is high in salt and organic contents. Excessive salt in the soil will eventually cause the fields to be incapable of growing crops. Hence, desalination of food processing wastewater is necessary.

In this project, we developed two dimensional nanostructure-based membranes for desalination of food processing wastewater. Two dimensional nanomaterials, one atom thick, can significantly reduce membrane thickness and reduce membrane fouling and increase water permeability. To address this need and produce effective nanocomposite membranes, we used a combination of graphene family nanomaterials and transition metal dichalcogenides to provide both antifouling and foul release properties. We also worked with food processing facilities in Quincy, WA as wastewater sampling locations. Washington State Department of Ecology supported our efforts with food processing facilities. An investigation on the Qunicy industrial food processing wastewater effluent treatment and reuse has been reported in this study. Treatment experiments with different ultrafiltration (UF), nanofiltration (NF), and reverse osmosis (RO) membranes were conducted in a bench-scale, crossflow unit. Treatment efficiencies of different membranes were

reported in terms of total dissolved solids (TDS) removal, initial water flux, operating pressure, and flux decline due to fouling.

Results show that graphene oxide (GO)- molybdenum disulfide (MoS_2) nanocomposite membranes could be used for decreasing the TDS concentration of the Quincy industrial wastewater effluent to 500 mg/L required for irrigation usage. Further modification of the composite membrane (i.e., changing the ratio of GO and MoS_2 in the mixtures, increasing the amount of nanomaterials, etc.) could result in even higher TDS removal efficiency. Though the commercial RO membrane showed a maximum 95% TDS removal efficiency, water permeability through the RO membrane was very low and it was susceptible to fast-flux decline due to fouling. On the other hand, antifouling GO-MoS_2 composite membrane treated 3 times higher wastewater effluent volume than RO membrane before each wash cycle, which will result in less frequent wash intervals and minimize the operating costs. Overall, considerable TDS removal, high initial water flux, and low operating pressure of the GO-MoS_2 composites, thus enables high productivity at reduced operational costs. Furthermore, superior antifouling behavior of the nanocomposite NF membranes would require less frequent membrane wash and could be reused for a longer time. The results of this study will be useful for designing a membrane-based treatment system in the industries for producing high-quality effluent. This would enable industrialists to reuse and recycle the polluted wastewater effluent for industrial and irrigation purposes.

1. INTRODUCTION

While population and industrial growth, and escalating climate change in this century are creating tremendous stresses in food-energy-water (FEW) systems, communities need efficient usage of resources and waste materials in FEW systems to combat these challenges. Wastewater is one of the largest waste materials in FEW systems, which communities can recover and recycle for the use in the FEW cycle. In North America alone, communities generate 19 trillion gallons of wastewater each year (Sato et al. 2013). Although 75% of this wastewater is treated, communities currently reuse only 3.8% for agricultural or other beneficial purposes. The total amount of wastewater in North America is 42% of agricultural water withdrawals, indicating that wastewater could help decrease stress on fresh water supplies and groundwater withdrawal. Food processing wastewater is one of the largest sources of wastewater. Therefore, there is a critical need in developing engineering solutions for sustainable recycling of food processing wastewater in food-energy-water systems.

Washington is a leading producer of numerous crops and key supplier of food throughout the world. Agriculture and food processing industries are the cornerstones of economy of Washington and other industries depend on the food-production industry such as transportation, machinery, fertilizers, etc. However, the food processing industries in the arid climate of Washington are facing challenges due to climate change, water shortage and groundwater depletion. Changing weather patterns are creating stresses on water availability. Moreover, in Washington State, major source of water for food processing is groundwater. Hence, communities need alternative sources of water for sustainability of food processing industries in Washington.

Wastewaters generated from food processing industries are large quantities and can be alternative sources of potable water. Currently the design discharge of wastewater treatment are limiting the

production at food processing industries. Currently the industries use water to create food for human consumption. The industries discharge the process water to a treatment facility as wastewater. The food industries could increase production if the seasonal discharge or the cost of treatment did not limit the beneficial use. A beneficial reuse for the food-producing wastewater could be a source water for a water treatment facility or a combined process water and drinking water facility. So, the community could immediately use the full discharge by discharging the drinking water into the potable water system. This would eliminate the cost of a storage lagoon for seasonal discharge, the cost of purple pipe for reuse of water, and decrease the amount of water the community withdraws from the ground. This increase in production would mean an increase in job opportunities in Washington State and a decrease in energy costs to pump the water out of the ground.

The main challenge with the reuse of food processing wastewater for a potable water system is contaminants. Food processing wastewater is generally high in salt content leading to high rates of biofouling during treatment. Rapid development of membranes for nanofiltration, reverse osmosis, and forward osmosis (Pendergast et al., 2011) during the last few decades has shown that these processes are viable approaches for separating contaminants from water. However, the advancement of membrane technology is severely hampered by the long-standing problem of fouling, which is caused by the accumulation of foreign substances, such as salts, on membrane surfaces or inside pores (Zodrow et al., 2014; Li et al., 2004). Fouling can seriously deteriorate membrane performance by reducing water permeability, lowering product water quality, increasing energy consumption, shortening membrane life, increasing operating costs, and releasing chemical wastes into the environment. Thus, there is a critical need to focus on improving the antifouling properties of membranes for desalination of food processing wastewater.

One promising approach for improving the antifouling properties of membranes is the use of nanotechnology. Rapid advances in nanotechnology have resulted in numerous nanomaterials with properties that are potentially useful in membrane processes. Among these nanomaterials, two dimensional nanostructures have emerged with numerous and unprecedented properties that can make state-of-the art membranes resistant to fouling (Geim and Grigorieva, 2013; Wang et al., 2012). Prior research has shown that two dimensional nanomaterials, one-atom thick (~1 nm), can significantly reduce the membrane thickness and membrane fouling (Zhang 2015). Hu et al. (2010) showed that graphene family two dimensional nanomaterials have both antibacterial and anti-corrosive properties. In addition, other two dimensional nanostructures called transition metal dichalcogenides, including molybdenum disulfide (MoS_2) and tungsten disulfide (WS_2), are highly hydrophobic and have extremely low friction, which can deter settlement of fouling agents and provide low adhesion of any fouling that may occur (Wang, Kalantar-Zadeh et al. 2012, Heiranian, Farimani et al. 2015). Our results confirm that both graphene oxide and molybdenum disulfide demonstrate provide superior antifouling properties.

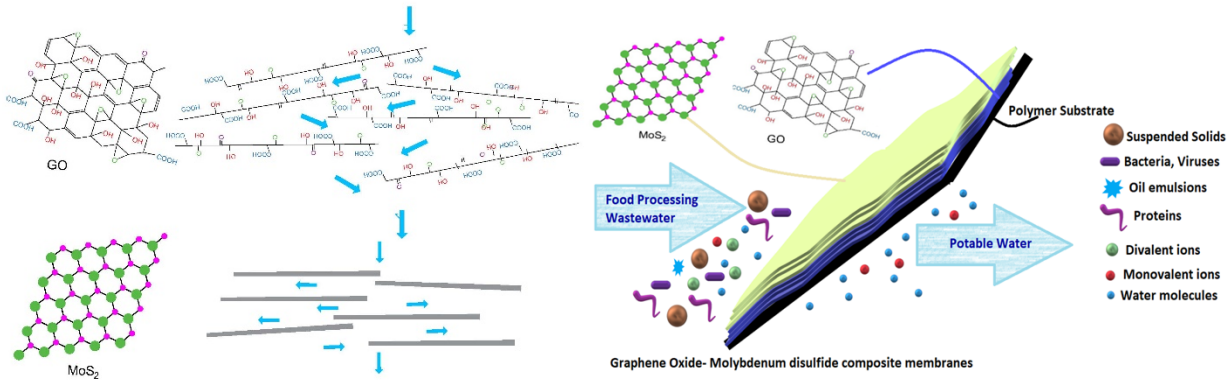

Figure 1. Thin film Graphene-Transition metal dichalcogenides (TMDCs) multi-functional membranes for wastewater treatment. The high level of oxygen functional groups on the basal plane of graphene oxide are prone to swelling and can also obstruct the water passage through the

nanochannels. Absence of functional groups on TMDCs provide an additional advantage in stability and help in fast water transport through its nanochannels. These modified thin-film nanocomposites would offer high salt rejection and antifouling performance maintaining fast water transport.

By combining the properties of both graphene family nanomaterials and transition metal dichalcogenides, we developed the creation of advanced antifouling membranes that can simultaneously provide low adhesion and antifouling capabilities. The overall objective of this project is to develop membranes for desalination of food processing wastewater. Figure 1 presents the overall schematic of our membrane development process. Based on our prior work, we have developed a combination of graphene family nanomaterials and transition metal dichalcogenides that will provide antifouling properties to nanocomposite membranes. We have utilized food processing facilities in Quincy, WA as wastewater sampling locations to test the membranes with alternative sources of food processing wastewater.

2. BACKGROUND

While the global population quadrupled, the world water demand was increased by seven times since the last century (Pendergast and Hoek 2011). The global water demand will continue to climb and would result in an increase of 20-30% above the present level of water use by 2050 due to the rising demand in the domestic and industrial sectors (WWAP 2019). There is no doubt that domestic, agriculture, industry, and energy demands on water resources would be growing even faster than never before (Bouman 2007). The United Nations World Water Development 2019 Report states that over 2 billion people experience high water stress, while 4 billion people face

severe water shortage at least one month of the year (WWAP 2019). Better water treatment technology is required not only to protect the existing freshwater resources but also to develop new water resources for meeting the world's growing demand (Pendergast and Hoek 2011).

Membrane-based water treatment technologies are becoming increasingly popular for seawater desalination, industrial wastewater recycling, and drinking water treatment applications (Hilal, Al-Zoubi et al. 2004). Membrane separation is one such treatment technology that selectively separates contaminants from water by retaining particles larger than its pore size. Contaminants with a smaller diameter than the rated pore size either pass through the membrane or may be captured by other mechanisms within the membrane structure. In addition, pressure-driven membrane processes, other separation processes like gas separation, pervaporation, and electrochemical membranes processes are also getting attention for industrial and environmental separations (Ulbricht 2006). Membrane-based separation offers high-quality effluent, fast installation and easy modification efforts, and requires less footprint to operate compared to the conventional water treatment processes. The applications of membranes range from large, utility-scale installation, to small point-of-use systems in homes (Karagiannis and Soldatos 2008, Sobsey, Stauber et al. 2008). Membranes are preferred over other water treatment technologies, such as disinfection, distillation, and media filtration, as they require no chemical additives, thermal inputs, or require surface regeneration of the used media (Pendergast and Hoek 2011). However, the advancement of membrane technology is severely hampered by the long-standing problem of fouling. Accumulation of foreign substances on membrane surfaces or inside pores causes fouling. Fouling deteriorates the performance of the membrane by lowering water permeability and also responsible for poor product water quality, increased energy consumption, short membrane life, etc. (Li and Elimelech 2004, Zodrow, Bar-Zeev et al. 2014). Biofouling, colloidal fouling, organic

fouling, and scaling remain the most significant problems for the efficient application of nano-filtration and reverse osmosis (Nguyen, Roddick et al. 2012, Ruiz-García, Melián-Martel et al. 2017). Many surfactants such as sodium dodecyl sulfate (SDS), poly(oxyethylene) isooctyl phenyl ether and oxidizing agents, such as hydrogen peroxide (H_2O_2), are used for membrane cleaning (Madaeni, Rostami et al. 2010). Chemical cleaning depends on a lot of parameters such as duration, temperature, shear stress, and pressure, which are difficult to control in operating condition. Moreover, depending on the fouling type different cleaning agents are required (Beyer, Laurinonyte et al. 2017). Therefore, there is a critical need to mitigate membrane fouling for effectively using the membrane-based treatment. Considerable efforts have been made in the past few years to modify polymeric membranes with different antifouling nanomaterials (Pramauro, Prevot et al. 1998, Bianco Prevot and Pramauro 1999, Lin and Murad 2001, Bahnemann 2004, Akhavan and Ghaderi 2010, Hoek, Pendergast et al. 2014, Perreault, Tousley et al. 2014, Chowdhury, Mansukhani et al. 2015). Fouling has been one of the significant drawbacks of the membrane-based treatment, antifouling performance evaluation of some commercial and lab-prepared membranes has been investigated besides their rejection performance.

The main objective of this study is to investigate the TDS removal efficiency of the some commercial NF, UF, and RO membranes and as well as one lab prepared GO-MoS_2 nanocomposite membrane. A systematic study was needed to identify the potential application of membrane-based food processing wastewater effluent treatment. Membranes were evaluated with respect to TDS removal efficiency, initial water flux, operating pressure, and their antifouling performance.

3. PROBLEMS

Wastewater recycling has become a trend to meet the rising global water demand for beneficial purposes such as irrigation, industrial processes, groundwater replenishing. (Grant, Saphores et al.

2012). Planned recycling of industrial wastewater can contribute significantly to the reduced withdrawal of freshwater from the system (Tong and Elimelech 2016). The ability to treat salty wastewater in a cost-effective and environmentally sustainable manner is critical to the food, drug, and chemical industries. Discharge of salty wastewater poses a severe risk to aquatic life (Cañedo-Argüelles, Kefford et al. 2018), influences nitrogen removal efficiency in wastewater treatment plants (Glass and Silverstein 1999, Campos, Mosquera-Corral et al. 2002) and markedly increases the emission of the greenhouse gas nitrous oxide (N_2O) from the plants (Tsuneda, Mikami et al. 2005). In addition, for irrigation purposes, total dissolved solids concentration needs to be less than 500 mg/L (~Electrical conductivity of 0.78 mmhos/cm) (Landschoot 2014). Conventional industrial wastewater treatment/management practices can hardly remove salts from water to reuse in irrigation and other industrial processes (Angelakis and Snyder 2015). Membrane-based separation processes (e.g., Reverse/forward osmosis) are becoming popular for removing salts from industrial wastewater, which can even achieve 100% resource recovery by zero-liquid discharge (ZLD) (Mays 2007, Oren, Korngold et al. 2010, Muhammad and Lee 2019). On the other hand, UF and NF membranes may not attain ZLD, but can certainly remove the maximum amount of contaminants and salts from water before discharge (Jiraratananon, Sungpet et al. 2000, Lau and Ismail 2009, Coskun, Debik et al. 2010). UF/NF incorporated into the industrial treatment processes can produce water that can be recycled and reused.

Fouling has been the major drawback of membrane-based water treatment. Membranes suffering from biofouling, organic, and inorganic fouling during operation, lead to poor product water quality and require frequent wash and sometimes replacement. The development of novel strategies for fouling prevention has been a long-active area in membrane research (de Lannoy, Jassby et al. 2013). Though commercial polymeric membranes such as polyamide (PA),

polysulfone (PSf), and polyethersulfone (PES) show excellent rejection, wide range pH tolerance, and chemical stability, they suffer greatly from fouling due to their hydrophobic nature (Sagle and Freeman 2004, Mi and Elimelech 2010, Shin, Kim et al. 2011, Gu, Jun et al. 2012, Liu and Mi 2012). So, the antifouling performance of the commercial and GO-MoS_2 composite membranes was systematically investigated besides their TDS rejection performance.

4. MATERIALS AND METHODS

4.1 Selection of membranes

The membrane-based treatment has been proposed to remove the TDS from the Quincy Industrial water. The performance of three different commercial membranes and a lab-modified nanocomposite membrane was investigated. The details of the membranes are included in Table 1:

Table 1: List of membranes used for TDS removal

Membrane type	Pore size (nm)	Membrane material
Ultrafiltration (UF)	30	Polyethersulfone (PES)
Nanofiltration (NF)	~ 2.5 nm (~600-800 Da)	Polyamide (PA)
GO-MoS_2 nanocomposite NF	3.84	Graphene oxide (GO) and Molybdenum disulfide (MoS_2)
Reverse Osmosis	N/A	Cellulose Acetate (CA)

A modified Hummers' Method was used to prepare the GO (Duch, Budinger et al. 2011, Chowdhury, Duch et al. 2013). MoS_2 was prepared using a lithium intercalation method as described previously (Lanphere, Luth et al. 2015). Hydrodynamic diameter (D_h) and zeta potential

(ζ-potential) of the materials were measured using a Zeta Sizer Nano ZS (Malvern Instruments, Worcestershire, U.K.) as described in previous articles (Childress and Elimelech 1996, Chowdhury, Duch et al. 2013, Lanphere, Luth et al. 2015, Esfahani, Languri et al. 2016).

4.2 Thin-Film Selective Layer Synthesis

Commercially available PES membranes were modified by GO, and MoS_2 by vacuum filtration to produce a uniform functionalization layer (Figure 2). First, the PES membrane was soaked in water and subsequently NaOH to activate the membrane. To prepare the functionalized membranes, 5 mg/L of GO in 25 mL DI water or 5 mg/L MoS_2 in 25 mL ethanol/water (45/55 vol%) was sonicated for 10 min, followed by the vacuum filtration of the diluted solution onto the PES substrate. In the case of the composite membranes, three types of modifications were performed. First, for the LBL assembly, 12.5 mL of 5 mg/L GO was filtered through the PES membrane and the membrane was air-dried for 12 h. Then 12.5 mL of 5 mg/L MoS_2 was vacuum filtered on top of the already deposited layer of GO and further dried in an oven before use. This GO-MoS_2 hybrid membrane was denoted as LBL-1. The second approach (LBL-2) was like the first, except that MoS_2 was deposited first, followed by the GO. For the composite mixtures of GO and MoS_2 (CM), two dispersions of GO and MoS_2 containing varying wt% of the materials were mixed by 15 min sonication and then the mixture was filtered onto the PES substrate. The composition details of the fabricated membranes are listed in Table 1. Following vacuum filtration, all membranes were kept in an oven at 50°C for 2 h for drying and then stored at room temperature for 24 h before use. In addition, commercial NF, and ultrafiltration (UF) membranes from different manufacturers were purchased from Sterlitech to compare the performance of the modified membranes.

4.3 Cross-flow filtration set-up

A CF016A crossflow assembly (Sterlitech, Kent, WA) was used for this study (Figure 1) (Alam, Guiney et al. 2020). The filtration unit has an effective membrane surface area of 20.6 cm^2 and can withstand pressures up to 400 psi. During operation, a pressurized feed stream (12.4 bar at 1.5 LPM flow rate) was passed over the membrane. This feed stream was separated into a permeate and a retentate stream. The former was collected to measure flux and rejection, while the latter was recycled to the feed stream. A digital weight scale was used to collect the water at fixed time intervals to measure the pure water flux of the modified membranes.

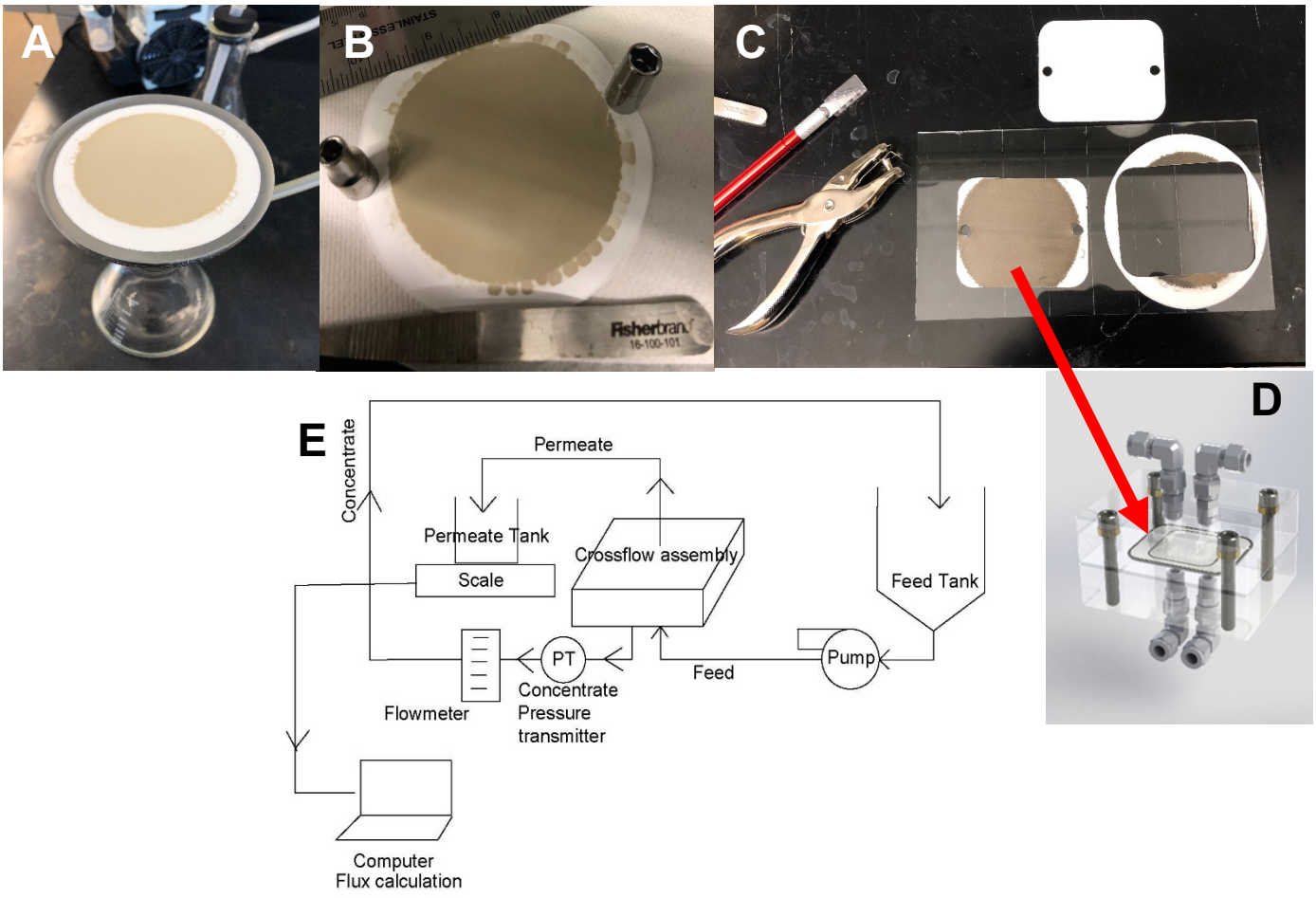

Figure 2: A) Nanomaterial suspensions were vacuum filtered onto PES membranes with a pore size of 0.03µm, retaining 100% of the nanomaterials on top of the substrate. B) Functionalized

membranes were thermally treated at 60°C and then kept at room temperature overnight. The modified membranes were cut to the desired sizes to fit into the cross-flow assembly (C & D). E) Schematic of the crossflow assembly used for the fouling studies.

GO-MoS_2 nanomaterials were vacuum filtered onto a PES substrate first and then were placed into the system (Figure 2A-D). All the commercial membranes were placed directly in the cross-flow assembly (Figure 2D) and the system was equilibrated till a stable water flux was achieved.

4.4 Characterization of materials and membrane

4.4.1 Electrokinetic and hydrodynamic characterization

Zeta Sizer Nano ZS from Malvern Instruments, Worcestershire, U.K. was used to determine the zeta (ζ) potential and size (D_h) and of the GO and MoS_2 nanosheets.(Childress and Elimelech 1996, Lanphere, Luth et al. 2015). The instrument is equipped with a He-Ne laser that had a fixed 633 nm wavelength and uses the Stokes-Einstein equation for calculating the average size (Elimelech, Gregory et al. 2013). Zeta potentials of the nanosheets were also measured using the same instrument. For potential calculations, the instrument uses dynamic light scattering (DLS) for determining the electrophoretic mobility of charged particles (Bouchard, Ma et al. 2009). ZetaSizer Nano ZS is programmed to use the Smoluchowski equation to calculate the zeta-potential from the electrophoretic mobility (Elimelech, Gregory et al. 2013).

4.4.2 XPS analysis and SEM imaging

XPS samples were prepared and analyzed using an ESCALAB 250Xi (Thermo Scientific) following a similar procedure as described previously published work (Hou, Chowdhury et al. 2015, Alam, Guiney et al. 2020). 5 mg of each sample was vacuum filtered onto a 0.1 μm PTFE membrane. The deposited film was left to settle for 15 minutes followed by rinsing and drying in DI water and air, respectively. XPS was also used to determine the surface composition and chemistry of the modified membranes using a procedure similar to previously published work (Hou, Chowdhury et al. 2015).

SEM Tescan Vega3 with EDAX capability was used to investigate the surface morphology and cross-section of the modified and unmodified membranes. Membranes were cut into small pieces and placed on the sample stubs using conductive carbon tabs. To avoid charging artifacts during imaging a gold coater (Technics Hummer V Sputter) was used for coating the SEM samples with a 5 nm conductive layer of gold. Thickness was controlled by manipulating the time and voltage. 3 min at 10 milliamps resulted in a coating thickness of approximately 7-10 nm on top of the samples. For the thickness measurements, the membranes were cut into small pieces and submerged in liquid nitrogen for the 60-90s. The frozen membranes were cleaved and kept in the desiccator to dry completely followed by sputter-coated before imaging.

Transmission electron microscopy (TEM) was used to determine the thickness of the deposited nanomaterials onto PES substrate. Before TEM analysis, membranes were cast into SPURR resin for a week and then cured in an oven for overnight. After that, the cured membranes embedded blocks were microtomed (Leica Reichert Ultracut R ultramicrotome) to 50 nm slices before being analyzed under TEM.

4.4.3 Contact Angle Measurement

The hydrophilicity of unmodified and modified membranes was evaluated using the contact angle (CA) analysis. Droplets of 2 μL were brought into contact with the membrane surface, and a side view image was taken immediately using a Data Physics OCA15 Contact Angle Analyzer. 2 μL droplets were brought into the contact of the membrane surface, and images were taken immediately to measure the water contact angles of the modified membranes. At first clean SiO_2 wafers were coated with 0.02 mg mL^{-1} GO, rGO, and MoS_2 dispersions (25 μL). Water droplets of 2 μL were injected onto the surface of interests, and the water contact angles were measured immediately. 5 replicates were taken from different areas of each membrane.

4.4.4. Pore Size Determination

Altered pore size *(r_m)* of the modified membranes was determined from the Gueroute Elforde Ferry equation(Wu, Gan et al. 2008):

$$r_m = \sqrt{\frac{[(2.9 - 1.75 * \varepsilon)(8 * \mu * \zeta * Q_w)]}{(\varepsilon * A_m * \Delta P)}} \qquad (1)$$

where ζ is the membrane thickness including the thickness of the deposited nanosheets (m), Q_W is the water flux ($m^3\ s^{-1}$) after 24 h equilibration at constant operating pressure (7 bar), A_m is the active membrane area (m^2), μ is the water viscosity (Pa. s), Δ*P* is the applied pressure (MPa), and ε is the membrane porosity that was determined using the following equation(Vatanpour, Madaeni et al. 2012):

$$\varepsilon = \frac{\omega_1 - \omega_2}{A_m * \zeta * dw} \quad (2)$$

where ω_1 and ω_2 are the weight of the wet and dry membrane respectively, and *dw* is the density of water (998 kg m^{-3}).

4.5 Water flux and TDS removal performance evaluation

The TDS removal and water flux of the membranes were evaluated using the cross-flow assembly. Prior to any measurement, the membrane was compacted with pure water at a pressure of 12.4 bar for 24 h in order to achieve a steady-state condition. The pure water flux rejection of each membrane was evaluated in this study. All filtration experiments were conducted at room temperature. Water flux of the commercial and lab-prepared membranes was determined in terms of equilibrated pure water flux ($Lm^{-2}h^{1}$). The equilibrated water flux and wastewater flux were calculated using the following equation:

$$J_{o}=\frac{M}{A_{m}*\Delta t}$$

where M is the weight of the permeate pure water (kg) and Δt is the permeation time (h). The TDS removal, R (%), of the membranes, was determined using the equation:

$$R=\left(1-\frac{C_P}{C_f}\right)*100\%$$

where *Cf* and *Cp* are the salt concentration in the feed and permeate solution, respectively. A bench conductivity meter (ThermoFisher Scientific) was used to measure the salt concentration in the feed and permeate solution. Then using a factor of 0.67, the conductivities of the solutions were converted to TDS. For the experiment, Quincy industrial wastewater was used as the feed solution at an operating pressure of 12.4 bar.

4.6 Antifouling performance of the membranes

Before each fouling experiment, the membranes were equilibrated for 24 h until a stable pure water flux (J_0) was attained. The flux decline was determined for all the membranes against the feed wastewater. Before any fouling experiment, the water flux was re-equilibrated to 180 $Lm^{-2}h^{-1}$ by adjusting the pressure to eliminate all other factors that can account for the flux decline of the membranes except fouling. Fouling experiments with NF and GO-MoS_2 composites NF were run at 12.4 bar with a feed rate of 1.6 L min^{-1} and for UF and RO membrane the applied pressures on the system were 10 bar and 17.5 bar respectively. However, even under that much high pressure, the water flux of the RO membrane was only 55 $Lm^{-2}h^{-1}$. The initial low flux of the RO membrane could result in less flux decline as it has been reported that the membranes with high initial flux suffer higher flux decline during fouling study.(Seidel and Elimelech 2002) The experiments were carried out at 20.5 ± 1 °C. The flux during the fouling study was calculated using the same equation as pure water flux. The normalized flux decline (J_B/J_{B0}) was calculated, where J_{B0} is the flux at the beginning of the fouling study and J_B is the flux calculated at 5 min intervals during the fouling study. Flux decline was reported as a function of total permeate volume. When the permeate flux of the membranes declined to 30% of the initial flux, the membranes were cleaned for 15 min with 500 mg/L sodium hypochlorite (NaOCl) followed by 5 min DI water wash. During the wash, the valve connected to the permeate side remained closed and the cleaning solution was only allowed to flow across the membrane top surface. The 2nd cycle of the fouling study was conducted similar to the 1st cycle.

The flux recovery ratio (FRR) was used to analyze the fouling resistance and regeneration efficiency of the modified and unmodified membranes. The FRR was evaluated using the following equation:

$$FRR = \left[\frac{J_R}{J_0}\right] * 100\%$$

5. Pressure-driven Water Transport Behavior and Antifouling Performance of Two-Dimensional Nanomaterial Laminated Membranes

Both GO (Figure 3B) and rGO (Figure 3C) create a dense layer on top of the PES substrate. GO rGO and MoS_2, which are large (laterally), coat the surface and might obstruct the pores (100 nm) of the PES. TEM images (Figure 3) also reveal that the thickness of the vacuum filtered GO, rGO, and MoS_2 nanomaterials varied from 9-15 nm, 15-25 nm, and 9-12 nm respectively. Moreover, the high rigidity of MoS_2 due to the presence of three atomic layers and high surface smoothness due to the lack of functional groups lead to a neatly packed membrane structure (Wang and Mi 2017). Functional groups in the GO and rGO structure could affect the laminar stacking of the materials and lead to an uneven surface during deposition (Figure 3B and 3C).

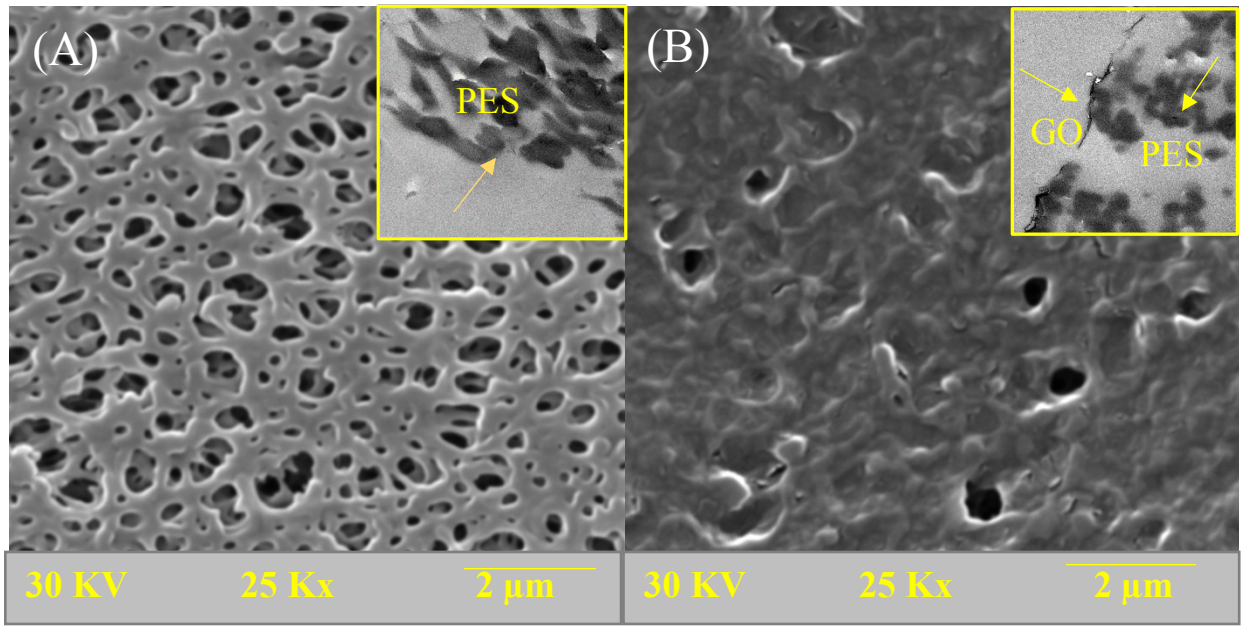

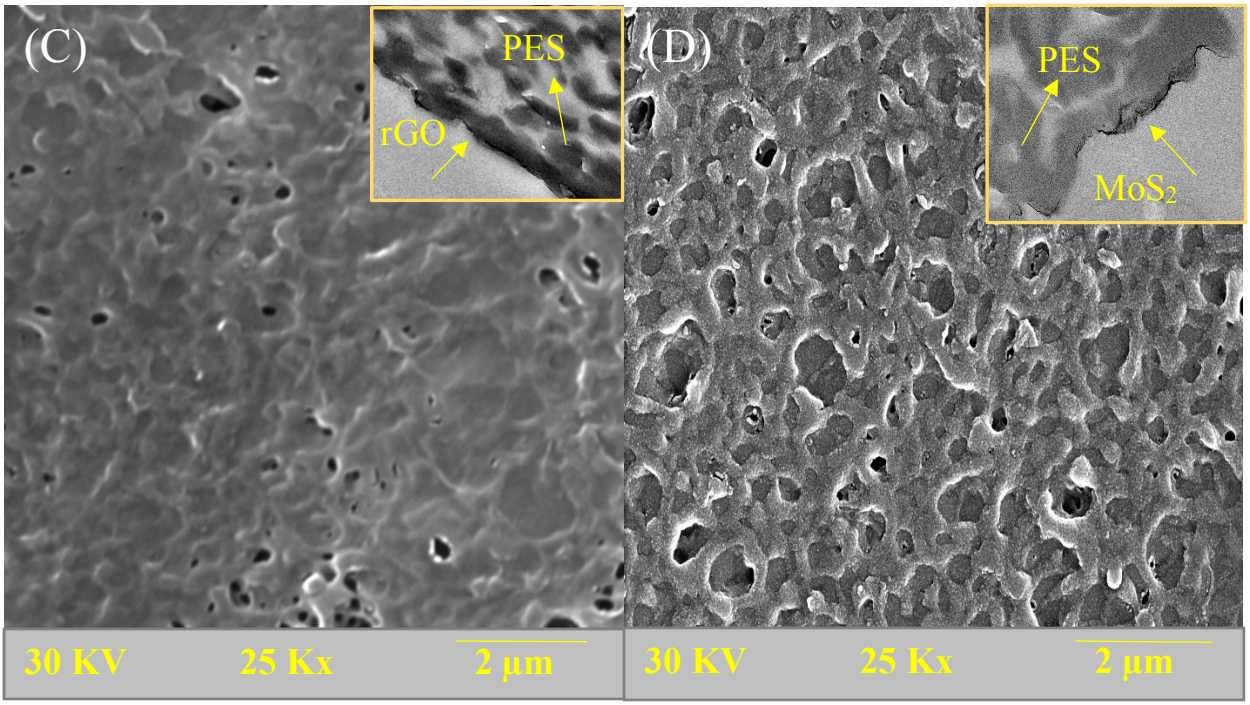

Figure 3: SEM and TEM characterization of (A) PES membrane support, (B) GO/PES, (C) rGO/PES, and (D) MoS_2/PES membranes. MoS_2 nanosheets create a smooth layer (9-12 nm) maintaining the original surface morphology of the PES membrane support. Both GO (9-15 nm), and rGO (15-25 nm) create a dense layer on the PES substrate during vacuum filtration causing pore blockage of the PES membranes.

5.1 Water flux of modified membranes

Figure 4A indicates that among the modified membranes, MoS_2/PES showed the highest water flux of 537 L m^{-2} h^{-1} while the flux of the GO/PES and rGO/PES membranes were 3.3 and 1.2 times lower than the MoS_2/PES membrane, respectively. The laminar structure of MoS_2 could attribute to the observed high water flux. Previously, it has been shown that the overlapping of the laminar MoS_2 nanosheets by vacuum filtration results in gaps allowing high water permeation (Sun, Huang et al. 2013, Heiranian, Farimani et al. 2015, Wang, Tu et al. 2017, Li, Sun et al. 2018).

These nanochannels formed by the MoS_2, are both smooth and rigid, lowering the hydraulic resistance (Wang, Tu et al. 2017) and energy barrier (Heiranian, Farimani et al. 2015). GO is highly decorated with oxygen-containing functional groups on its structure, which could block those nanochannels, resulting in low water permeability (Wang, Tu et al. 2017). When these oxygen-containing functional groups are removed from the basal plane by a reduction process (rGO), the permeability of the film increases by 63%. Reduction of GO to rGO could make the rGO susceptible to less swelling and result in less obstruction of the pores. Pressure-assisted filtration could also be responsible for the low water flux of the GO functionalized membrane. The loosely packed GO nanosheets get compacted under pressure, and the extra transport channels are reduced to impede fast water transport (Chong, Wang et al. 2018). The rGO and MoS_2 membranes appear to be less susceptible to rapid compaction under pressure in this study. During 24h equilibration, the fast pure water flux decline (728 $Lm^{-2}hr^{-1}$ to 300 $Lm^{-2}hr^{-1}$) was noticeable within the first 3h on the GO membrane, whereas, the rGO (1500 $Lm^{-2}hr^{-1}$ to 952 $Lm^{-2}hr^{-1}$) and MoS_2 (1340 $Lm^{-2}hr^{-1}$ to 911 $Lm^{-2}hr^{-1}$) showed slow flux decline over a period of 8h. In fact, the combination of rapid compaction under pressure and swelling behavior of GO could have led to the unstratified arrangement, which results in slow water transport. The highest pure water permeability (587.5 $Lm^{-2}hr^{-1}$) was observed for the unmodified PES membrane due to the unblocked pores.

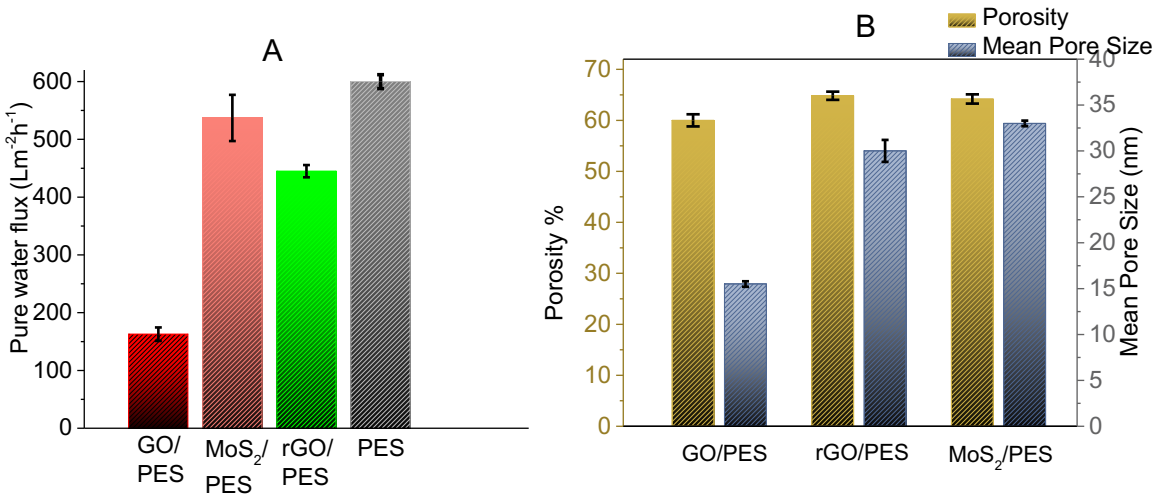

Figure 4: A) Equilibrated pure water flux of the modified GO/PES, MoS_2/PES, rGO/PES and unmodified PES membranes. B) The overall porosity and mean radius of the modified PES membranes. The pore size of all the membranes was reported in terms of equilibrated flux.

5.2 Porosity, pore size and rejection performance of the modified membranes

Both porosity and hydrophilicity play significant roles in the permeability and antifouling efficiency of the membrane (Gebru and Das 2017). The modified membranes show a porosity of 63-64%, indicating that the porosity does not differ significantly from the original PES membrane (~64%). Though the top surface of the PES membrane was covered by the thin layer of nanomaterials (9-25 nm), water can still diffuse through the GO or MoS_2 nanochannels over a 24 h period and maintain high porosity (Figure 4B) (Huang, Song et al. 2013, Wang, Zhang et al. 2016, Wang and Mi 2017, Wang, Tu et al. 2017). However, the inclusion of GO and MoS_2 has been found to be effective for increasing the porosity of the membranes in previous studies (Mukherjee, Bhunia et al. 2016, Zhu, Tian et al. 2016, Sri Abirami Saraswathi, Rana et al. 2017). GO/MoS_2 attracting more water inside the membrane matrix during the phase inversion might

have increased the membrane porosity in those cases (Mukherjee, Bhunia et al. 2016). However, a simple vacuum filtration was used to keep the nanomaterials exposed on the surfaces in this study and the water uptake by the nanochannels of the thin-layered materials was minimal. Moreover, water from the top surface of the wet membranes was further dried by the filter paper during the porosity measurement, which removed the water held by the nanomaterials. Figure 4B also shows that the pore size of the different membranes, calculated using Equation 3 where equilibrated (after 24 h) pure water flux was used, differed significantly even if the same amount of materials was deposited onto the substrate. The pore size of the GO/PES membrane was significantly smaller (~15.4 nm) than MoS_2/PES (~33 nm) and rGO/PES (~30 nm). Though Gueroute Elforde Ferry equation uses water flux to measure the pore size, it was used to predict the altered pore size of nanomaterial functionalized membranes in previous studies (Wu, Gan et al. 2008, Wang, Zhu et al. 2018). It was clear that the pore size of the laminated membranes atop 0.1 μm PES substrate was in the ultrafiltration (UF) range and could be used for albumin protein, virus, carbon black, and gelatin separation (Otaki, Yano et al. 1998, Lohwacharin, Oguma et al. 2009, Lin, Hu et al. 2018, Arumugham, Amimodu et al. 2019, Kim, Dehlinger et al. 2019).

Table 2: Foulants rejection and flux losses caused by total fouling (F_t), reversible fouling (F_r) and irreversible fouling (F_{ir}) on modified and unmodified membranes

Membrane	R_t	R_r	R_{ir}	Rejection
GO/PES	71±0.2%	17±1.1%	54±3.4%	66%
rGO/PES	79±0.7%	6±0.6%	72±2.3%	63%
MoS_2/PES	78±0.9%	43±1.3%	35±1.7%	65%
PES	92±1.2%	9±2.3%	83±0.6%	23%

All modified membranes with larger pore diameter than BSA (~2.6 nm) (Erickson 2009) and SA (~7 nm) (Dembczynski and Jankowski 2001) molecules still showed reasonable foulants rejection (Table 2) performance (63-66%), indicating that size exclusion was not the dominating mechanism for rejection. Both the modified membranes and BSA/SA are negatively charged in the experimental condition and therefore the foulants were most likely rejected from the membrane surface due to electrostatic repulsion (Bidsorkhi, Riazi et al. 2016, Sri Abirami Saraswathi, Rana et al. 2017). The build-up of the additional hydration layer near the hydrophilic membrane surfaces might also prevent the foulants from coming into contact with the surface, which results in higher rejection (Emadzadeh, Lau et al. 2014).

5.3 Fouling study

The anti-fouling ability of the membranes was assessed by determining the normalized flux decline (J_B/J_{B0}) during fouling with SWW. The average initial flux decline after fouling on GO/PES, rGO/PES, MoS_2/PES and PES membranes was 59±2%, 60±1.2% , 47±2.1% and 73±3.1%, respectively, as a function of permeate volume (250 mL) (Figure 5A), indicating that MoS_2/PES was less prone to fouling in this case. Significant initial flux decline of GO, rGO, and PES membranes demonstrate that foulants deposition rate was higher on those membranes and MoS_2/PES membrane showed antifouling performance than others. Another key aspect of this finding was, unlike the PES membrane, the flux of the modified membranes reached a stable point after initial flux decline (Figure 5A). In addition, flux decline during fouling study was ~1.5 times slower on the MoS_2 membrane than PES membrane, which indicates the MoS_2 membrane can be operated for a longer time without requiring frequent wash than the unmodified membrane. The high amount of organic matter present along with the diverse salt chemistry makes the SWW a

more complex environment. The absence of a conjugated structure in MoS_2 could help avoid the problem of mineral scaling and organic fouling (Wang and Mi 2017). On the other hand, because of divalent cation-π, π-π, and electrostatic interactions, GO, and other graphene-based membranes suffer severe mineral scaling, especially $CaCO_3$ and $CaSO_4$ (Ray, Tadepalli et al. 2015, Wang and Mi 2017). Slightly higher FRR provides another advantage of the MoS_2/PES and GO/PES membranes over the rGO/PES and PES membranes (Figure 6B). High FRR of MoS_2 membranes suggests that it would require less frequent wash intervals than PES or rGO membranes. The high/low flux recovery is directly related to the reversible/irreversible fouling occurring on the respective membranes.

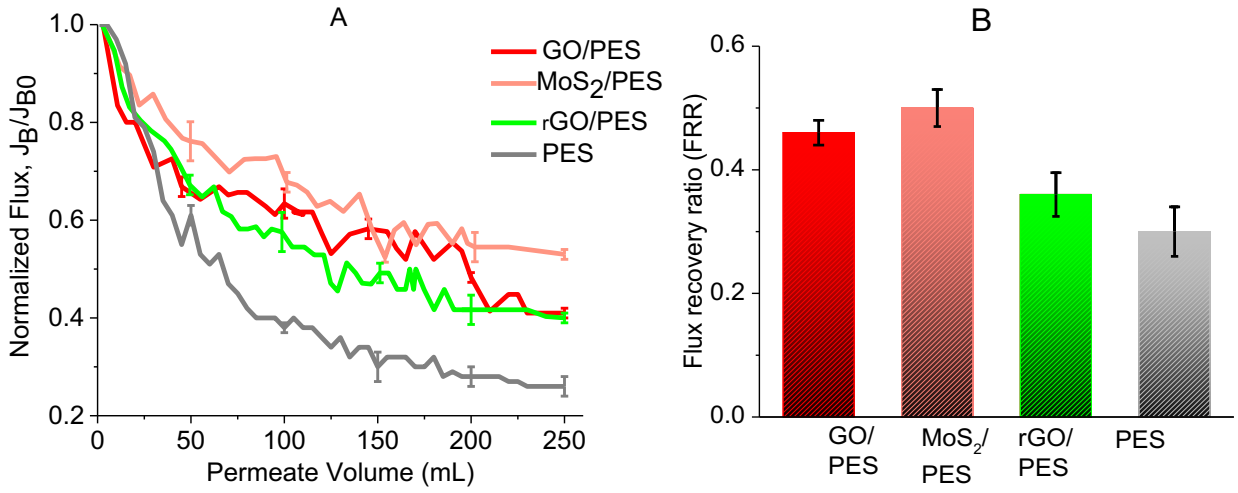

Figure 5: A) Normalized flux decline (J_B/J_{Bo}) of modified and unmodified PES membranes during the fouling study with SWW. B) Flux recovery of unmodified and modified PES membranes after 2 h during the fouling study with SWW and 15 min DI water wash.

Table 3 shows that the MoS_2/PES surface was subjected to 43% reversible fouling while the GO and rGO/PES surfaces experienced 17% and 6% reversible fouling. High irreversible contamination on both the rGO and PES surfaces could be due to the hydrophobic nature of the rGO and complex polymer matrices of PES, which was not easy to release by a simple DI wash. Though the PES membrane used in this study is hydrophilic, as confirmed from the contact angle measurement (50.6°±1.85°), it still suffered from severe fouling mainly due to its conjugated π bonds.

Overall, from the fouling study, it is clear that the modified membranes demonstrate superior antifouling performance over commercially available PES membranes. Moreover, under severe fouling condition, MoS_2 functionalized membranes outperform GO and rGO membranes due to the absence of functional groups on its structure.

5.4 Summary

This work provides a deeper understanding of the pressure-driven water transport behavior and antifouling performance of some exciting 2D nanomaterials (Figure 6). Pressure-assisted filtration recognizes their potential for the membrane-based wastewater treatment in industries. Herein, a facile method to laminate PES membranes with various 2D nanomaterials using vacuum filtration is presented as the intention was to explore the surface chemistry of the nanomaterials on the propensity of fouling. Overall, all modified membranes showed improved antifouling performance over commercially available hydrophilic PES membranes. This assessment of the antifouling performance under simulated fouling conditions will contribute to future studies especially preparing membranes with MoS_2 as it is a relatively new material in this field compared to GO

and rGO. The functional groups in GO create a non-uniform surface during self-assembly and block the passage of water, which results in low permeability compared to MoS_2. A reduction in the oxygen-containing functional groups in rGO significantly improved the water flux, again indicating that the decrease in water transport is due to the presence of functional groups on GO during pressure-driven filtration. Apart from fast water transport, there are additional advantages of MoS_2 over the graphene-based materials. Functional groups in GO and rGO structure are more prone to scaling and organic fouling especially under harsh conditions due to their conjugated structure. Of the 2D materials that were tested, MoS_2-laminated PES membranes demonstrated superior antifouling performance while still maintaining high water permeability.

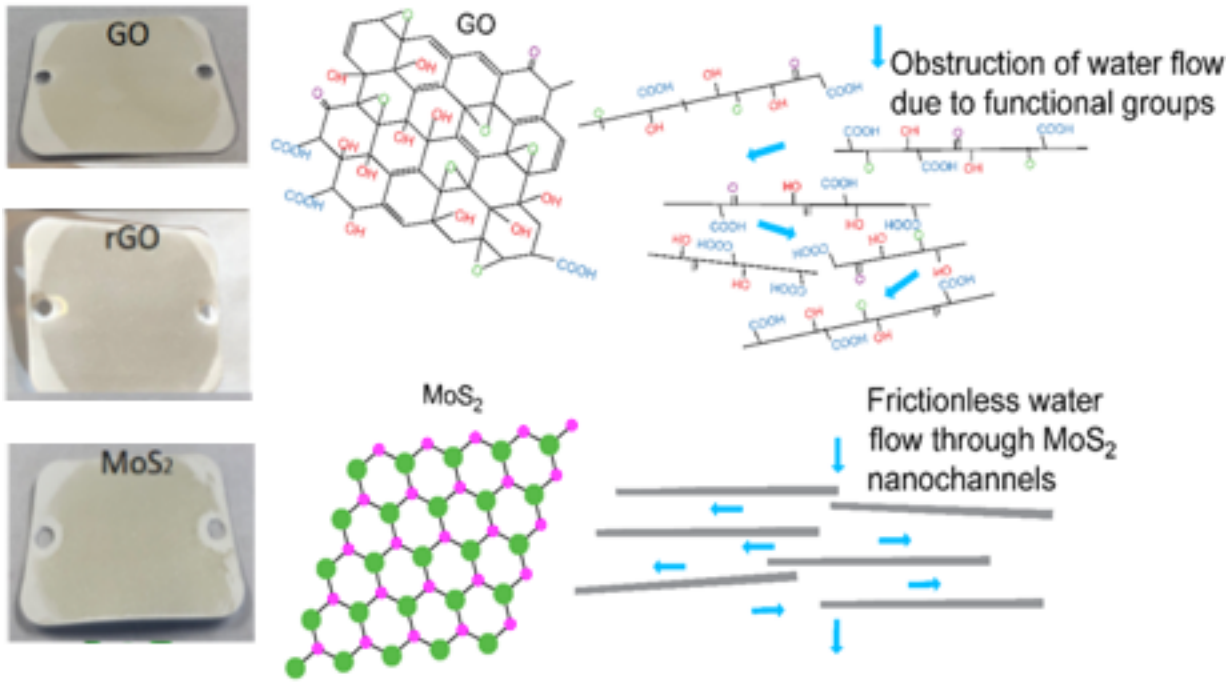

Figure 6. Schematic of mechanisms of GO and MoS_2 nanomaterial functionalized membranes

6. Performance Evaluation of Two-Dimensional Nanomaterial-Based Composite Membranes for Wastewater Reuse

6.1 Nanomaterials and Modified Membranes Characterization

The average hydrodynamic diameters of the nanosheets in deionized water were measured to be 385.3 ± 7.58 nm (GO) and 153.5 ± 1.67 nm (MoS_2). The zeta potentials of GO in deionized water was measured to be -43.33 ± 0.5 mV, which corresponds to mobility of -4.01 ± 0.04 μmcm/Vs and zeta potential of MoS_2 was -40.34 ± 0.76 mV corresponding to mobility of -3.16 ± 0.06 μmcm/Vs. As most of the foulants found in the environment are negatively charged, MoS_2 and GO modified membranes would decrease foulants attachment onto their surfaces due to electrostatic repulsion (Chen and Elimelech 2008), hence making them antifouling membranes.

Table 3. Preparation details of the fabricated membranes and their thickness

Membrane	GO wt%	MoS_2 wt%	Average thickness, μm	Porosity (%)	Contact Angle (°)
GO	100	0	0.78±0.13	88.5±0.2	40.1±2.8
MoS_2	0	100	0.61±0.21	89.5±0.3	57.9±5.6
LBL-1 (MoS_2 on GO)	50	50	0.99±0.1	86±0.1	57±5
LBL-2 (GO on MoS_2)	50	50	0.91±0.1	88.5±0.1	41±2.5
CM-1 (25:75 GO:MoS_2)	25	75	0.61±0.09	91±0.2	53.0±1.7
CM-2 (50:50 GO:MoS_2)	50	50	0.72±0.1	90±0.4	52.7±5.4
CM-3 (75:25 GO:MoS_2)	75	25	1.1±0.2	90±0.3	48.5±4.5

XPS results (Figure 7) of the C 1s region for membranes containing GO showed three convoluted peaks of O-C=O (288.5 eV), C-O (~286.8 eV), and C-C (~284.8 eV). For membranes functionalized with MoS_2, three characteristic peaks were seen in the Mo 3d region corresponding to the Mo $3d_{3/2}$ (~232.5 eV), Mo $3d_{5/2}$ (~229 eV), and S 2s (~226.5 eV) and the characteristic doublet peak (~162.5 eV) was observed in the S 2p region. XPS also elucidates the increasing ratio of MoS_2:GO in the membranes in the case of GO-MoS_2 composites. As the MoS_2 content increases in the composites, the C-C, C-O, O-C=O peaks diminish while the Mo $3d_{3/2}$ and Mo $3d_{5/2}$ peaks appear (Figure 7).

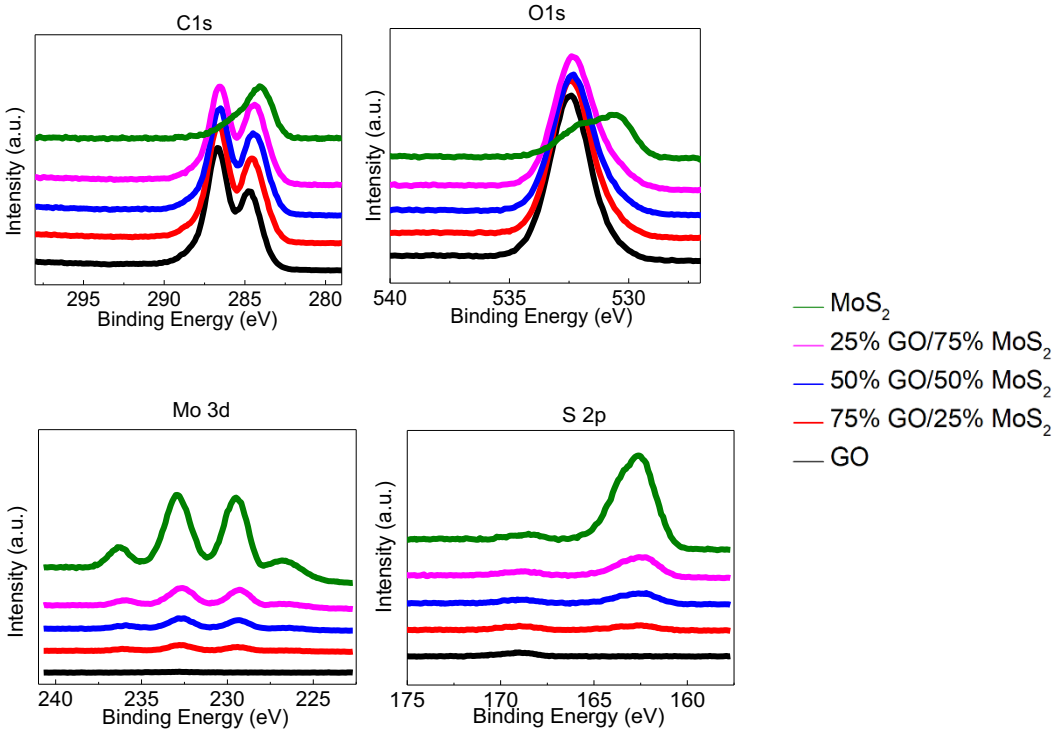

Figure 7: XPS spectra of PES membranes functionalized with GO, MoS_2, and GO-MoS_2 composites.

SEM images (Figure 8) of the modified membranes show their surface morphology and cross-section. GO nanosheets created folds on the surface of the PES substrate (Figure 3A), while MoS_2

membranes showed a granular morphology (Figure 8B). SEM images confirm that the active layers of the modified membrnes were completely covered with the nanosheets, which is critical for antifouling and rejection study. In the case of the composites, as MoS_2 content increases, the granular morphology became more pronounced on the surface (Figure 8C, D). This same trend in morphology can also be observed in the cross-sectional images. While a stacked-layer morphology is obvious in the cross-section of the MoS_2 membrane, this morphology is not observed in the GO membranes. The thickness of the active layer of the composites increased than the only GO or MoS_2 membrane (Table 3). This observation further indicates that the nanosheets intercalated between layers. CM-1 still holds the structure of pristine MoS_2 membrane facilitating the formation of nanochannels that offer fast water transport through the membrane.

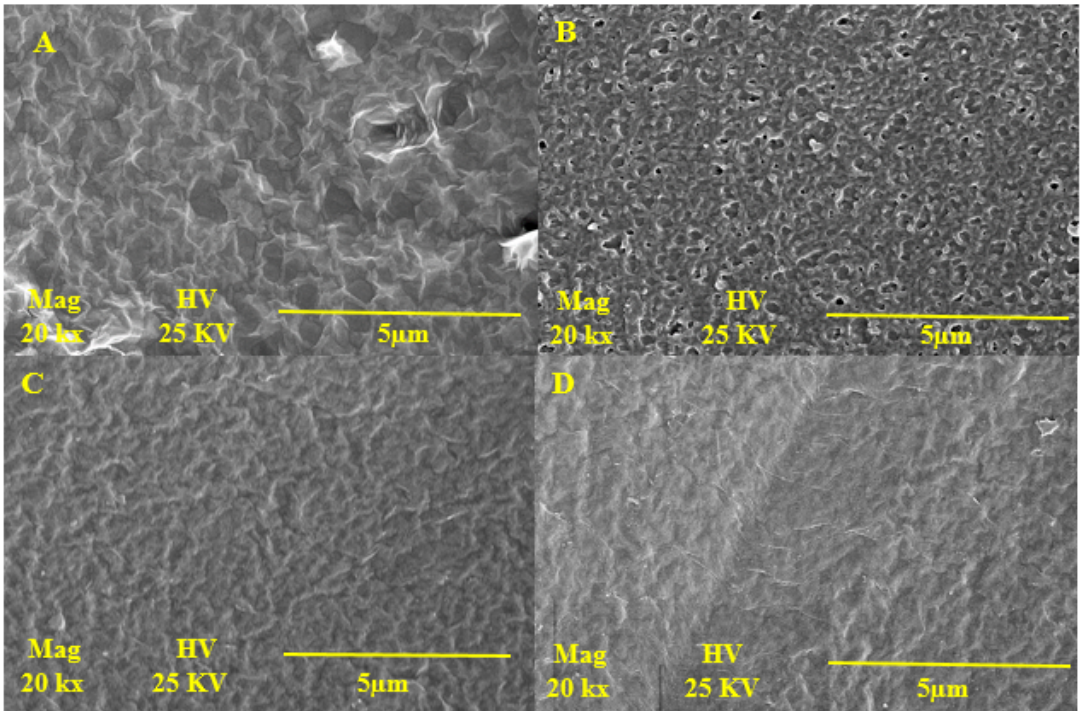

Figure 8: SEM images of the functionalized membranes: A) Surface of GO modified membrane; B) Surface of MoS_2 modified membrane; (C) Surface of GO-MoS_2 composite membranes CM-3, and (D) CM-1.

The altered porosity of the functionalized membranes were calculated using Equations 1. The porosity of all the membranes fell within the range of 86-92%. The porosity increased with the addition of MoS_2 (Table 3). The contact angle of the membranes increases with increasing ratio of MoS_2:GO in the membranes (Table 3) as a result of the hydrophilic nature of the GO. Thus, it is anticipated that GO functionalized membranes will offer faster water transport (Wang, Zhu et al. 2018).

6.2 NF Performance of the GO/MoS_2 Membranes

It is well-established that membrane permeability is directly related to the hydrophilicity and the microstructure of the membrane. Although the membranes with high GO content were more hydrophilic than MoS_2 (Table 3), the water flux of the MoS_2-modified PES membranes was 2.5-5 times higher than that of the GO-modified and composite membranes (Figure 9A). The laminated MoS_2 nanosheets could result in organized gaps and this attributes to the observed high water flux (Sun, Huang et al. 2013, Wang, Tu et al. 2017, Li, Sun et al. 2018). Smooth and rigid MoS_2 nanochannels lower the hydraulic resistance (Wang, Tu et al. 2017) and energy barrier (Heiranian, Farimani et al. 2015). On the other hand, the side-pinning effect of the oxygenated functional groups of GO affects fast water transport through its nanochannels (Wei, Peng et al. 2014, Zheng, Tu et al. 2017, Alam, Guiney et al. 2020). Incorporation of MoS_2 into a GO matrix results in higher water flux, which increases with the addition of more MoS_2 (Figure 9A). The slower water transport behavior in the presence of more GO further supports the argument that the water flux is decreased due to the side-pinning effect. On the other hand, the CM-3 composite (75 wt% GO/25 wt% MoS_2) showed the highest salt rejection performance with a slight decrease in water permeation rate compared to the GO membrane (Figure 9B). This observation is in accordance

with the 'trade-off' theory (Vrijenhoek and Waypa 2000, Han, Runnells et al. 2002) between permeability and rejection performance.

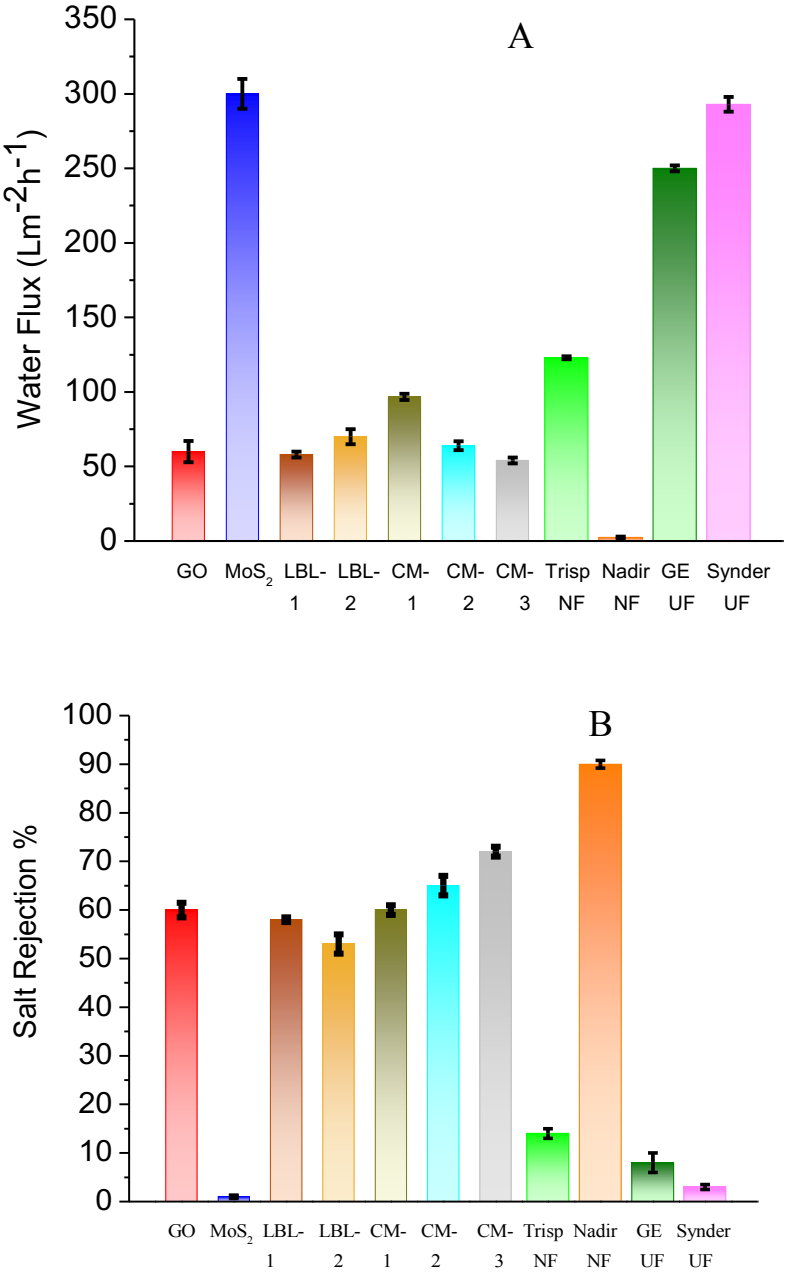

Figure 9: Comparison of pure water flux (A) and rejection (B) performance among the functionalized membranes and commercial membranes.

Due to the synergistic effect of the GO and MoS_2, the trade-off relation between rejection and flux has decreased. The CM-2 composite shows slightly higher salt rejection while maintaining a similar water transport rate compared to the GO membrane. Similarly, the water flux of the CM-1 membrane was 1.6 times higher than the GO membrane while maintaining a similar rejection rate. The Donnan exclusion mechanism, size exclusion, and non-swelling behavior could contribute to the improved performance of the GO-MoS_2 composites over the GO and MoS_2 coated membranes as will be discussed in the following section. Commercial NP010 (Microdyn Nadir^{TM}) showed better rejection performance than the composite membranes, but permeate flux dropped significantly from 54 $Lm^{-2}h^{-1}$ (CM-3) to 2.33 $Lm^{-2}h^{-1}$ (NP010) under the same operating conditions. On the other hand, SBNF (Trisep^{TM}) offered 2.5 times higher water flux, but it showed 22% less salt rejection than our CM-3 membrane. In addition, it can be seen that the water permeability and rejection behavior of the composite GO-MoS_2 membranes developed here were comparable with NF membranes reported in the literature. Considering the flux-rejection "trade-off" theory, it can be concluded that lab developed both LBL assembled and GO-MoS_2 composite (CM) membranes simultaneously offer high water flux and excellent rejection performance.

6.3 Antifouling Study

The antifouling performance of the membranes was assessed in terms of normalized flux decline (J_B/J_{B0}) after 6h fouling study with synthetic wastewater (SWW) solution. Figure 10 shows that the GO functionalized membranes were susceptible to fast-flux decline than MoS_2 functionalized membranes.

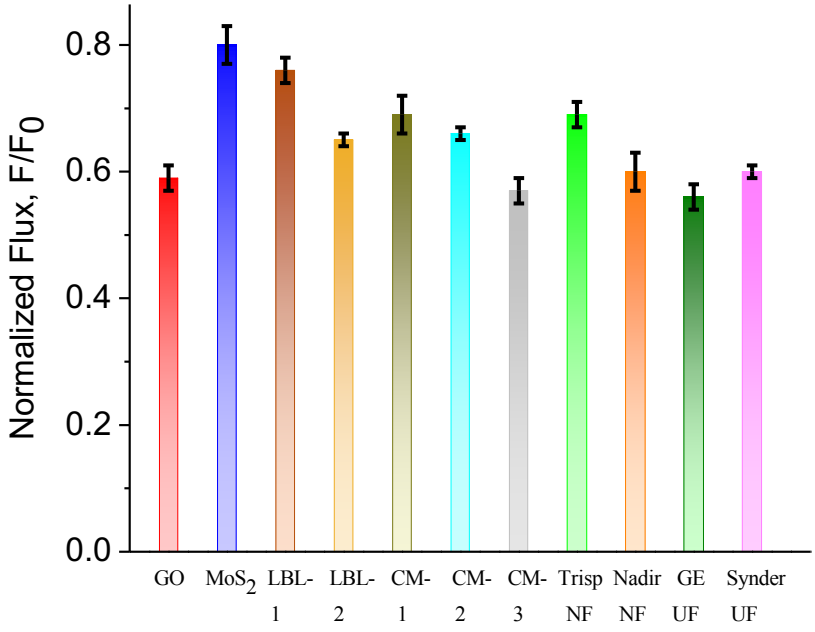

Figure 10: Normalized flux (J/J_0) of the modified and commercial membranes at the end of 6h fouling study with SWW.

Membranes with high GO content experienced the maximum flux decline. Furthermore, the flux decline of the GO and CM-3 membranes never reached equilibrium even after 6 h of fouling, whereas the other membranes that contained higher amounts of MoS_2 reached a stable flux after the initial decline. The MoS_2 coated membrane and LBL-1 (MoS_2 facing the feed side) membrane demonstrated the best antifouling performance of all membranes tested with the least flux decline (20-24%). The synergistic effect of MoS_2 and GO within the composites resulted in better antifouling performance than membranes functionalized with only GO. Higher MoS_2 content within the composite membranes leads to better performance overall. This trend in increased fouling due to higher content GO membranes can be attributed to the surface chemistry of GO. The hydroxyl, epoxy, and carboxyl functional groups of GO can interact with polysaccharide and proteins via hydrogen bonds, π-π interactions, and Lewis acid-base (Gao, Alemany et al. 2009, Hartono, Wang et al. 2009, Dreyer, Park et al. 2010). This leads to quick foulant layer formation

on GO membranes (Alam, Guiney et al. 2018), hence fast flux decline. On the other hand, lack of functional groups on MoS_2 results in lower interaction with the functional groups of polysaccharide and proteins (Alam, Guiney et al. 2018, Alam, Guiney et al. 2019, Alam, Guiney et al. 2020). Less foulants attachment on MoS_2 thus lead to least flux decline after 6h fouling study. MoS_2 functionalized membranes were also less prone to fouling than all the commercial membranes, indicating the superior antifouling performance of MoS_2 over polymeric membranes.

6.4 Summary

This work provides a deeper understanding of the filtration and rejection performance of some widely used 2D nanomaterials, namely GO and MoS_2 (Figure 11). Despite its hydrophilic nature, the functional groups in GO impede fast water transport, which results in low permeability compared to MoS_2. The frictionless flow of water through MoS_2 nanochannels improves the water transport of GO-MoS_2 composites while maintaining superior antifouling and salt rejection performance. In addition, unlike layer-stacked GO membranes that swells in presence of water, layer-stacked MoS_2 and GO-MoS_2 composite membranes demonstrate excellent anti-swelling properties. This aqueous stability is mainly due to the equilibrium between the short-range attractive van der Waals and repulsive hydration forces. The composite membranes developed in this study and commercial NF membranes showed comparable salt rejection, water flux, and better antifouling performance, which demonstrates their potential for the preparation of NF membranes.

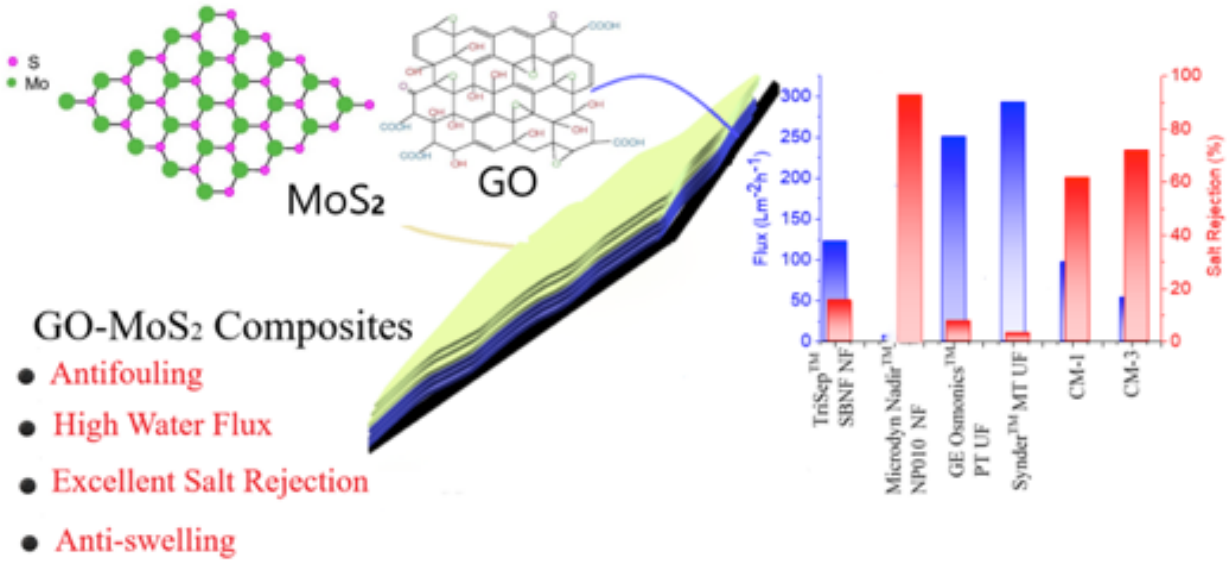

Figure 11. Schematic of mechanisms of 2D nanocomposite membranes.

7. Performance Evaluation of Two-Dimensional Nanomaterial Composite Membranes for Desalination of Food Processing Wastewater

7.1 Water flux of the membranes

The pure water flux of the membranes was determined at a constant pressure of 180 psi (Figure 12). The pressure. Among all the membranes, the UF membrane showed the highest water flux due to its larger pore size. The commercial NF membrane showed 1.5 times higher water flux than the lab-prepared GO-MoS_2 composite NF membrane. On the other hand, the RO membrane offered very low water flux at that pressure. Usually, the operating pressures for RO membranes range from 140-1450 psi due to their smaller pore sizes, which allow only water molecules to pass through while rejecting most of the ions present in the water. So, it was clear that the RO membrane would require considerably higher pressure than the other membranes to achieve a reasonable or comparable water flux to operate. Assuming the flow requirements of the membranes in the industrial set up may vary from 22 to 200 gallons per minute (GPM), we have calculated the

required area for all the membranes used in this study (Table 4). This would give an idea of how many channels/crossflow assemblies (configuration) would require to reach the target flow. However, it should be noted that the membrane areas would decrease or increase with the increase and decrease of the operating pressures, respectively. Usually, the filtration treatment system in the industry is designed in such a way that multiple cross-flow modules are connected in a series (Figure 2a), and inside each cylindrical cross-flow configuration, the spiral-wound membrane filter is rolled within the chamber with the help of spacers. Owing to the pressure drop, small spiral-wound modules consist of only one envelope (membrane area 1–2 m^2, membrane channel 2–5 m). (Basile, Gallucci et al. 2010) So, assuming the average membrane area inside each module 2 m^2, the number of cross-flow modules required for each membrane used in this study were determined and shown in Table 4.

Table 4: Membrane area required to achieve the industry flow requirements of 22-200 GPM

Membrane	Operating pressure (bar)	Membrane area required (m^2)	No of modules required
UF	12.4	20-185	10-93
NF	12.4	39-357	20-179
GO-MoS_2 nanocomposite NF	12.4	59-540	30-270
RO	12.4	628-5714	314-2857

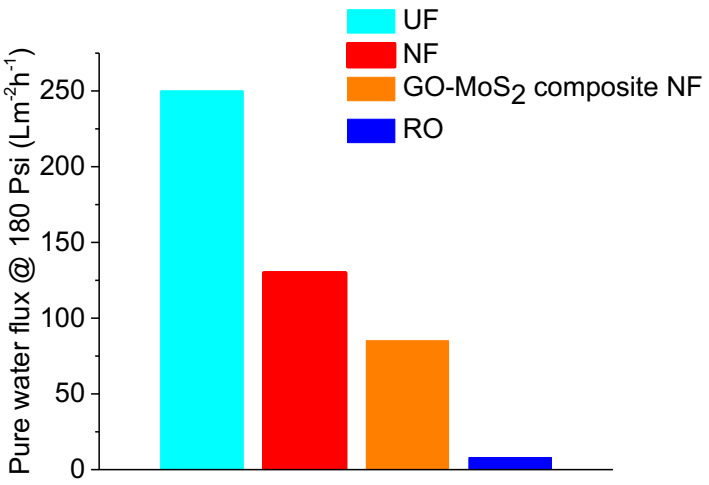

Figure 12: Pure water flux of the membranes at constant pressure (180 psi)

7.2 TDS removal performance

Figure 13 indicates that the RO membrane rejected about 95% TDS from Qunicy industry wastewater, which brought the TDS level from 1300 mg/L to 43 mg/L. Lab-modified NF membranes showed 8% higher TDS removal than the commercial NF membrane. Effluent TDS of the commercial NF and GO-MoS_2 composite NF was 618 mg/L and 548 mg/L, respectively. The lab-prepared NF membrane came close to achieve the effluent TDS concentration of 500 mg/L imposed by EPA. However, further modifications (i.e., increasing the GO content in the composite) could result in better TDS removal performance and bring the TDS level below 500 mg/L. Even though the UF membrane showed the highest water flux, its poor TDS removal performance makes it unsuitable for Qunicy industrial wastewater effluent treatment.

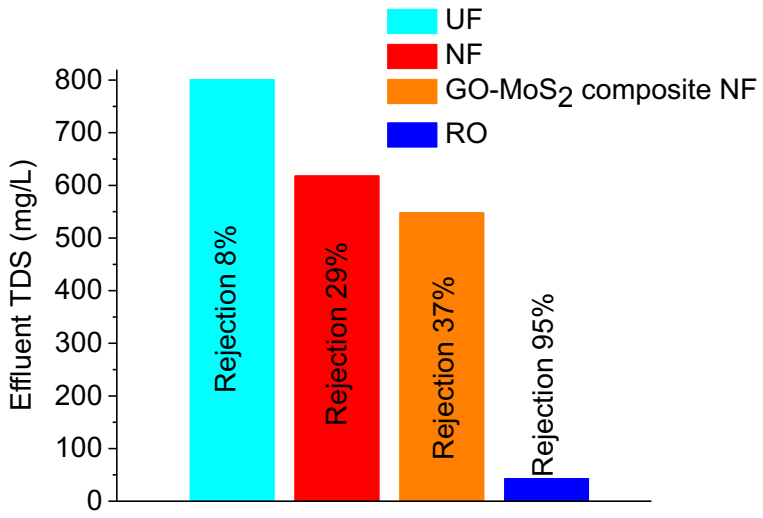

Figure 13: TDS removal performance of the membranes

7.3 Antifouling behavior of the membranes

Figure 14 indicates that the antifouling behavior of the GO-MoS_2 composite NF membrane outperformed the commercial membrane by quite a large margin. After the 1st cycle of the fouling study, the lab-prepared membrane suffered only 59% flux decline and produced a permeate volume of 386 mL. Whereas the second-best antifouling performing membrane, which was the UF membrane, delivered a permeate volume of 309 mL with a flux decline of 71%. The commercial NF and RO membranes performed even worse as they suffered a significant flux decline for achieving permeate volumes of 145 mL and 137.5 mL, respectively. In addition, the 2nd cycle flux decline behavior of the GO-MoS_2 membrane was identical to its 1st cycle of fouling study, while the other membranes showed a faster flux decline trend during the 2nd cycle of the fouling study. This indicates that the GO-MoS_2 membrane can be used for longer than commercial membranes without requiring frequent wash intervals. High negative surface charge, low surface roughness, and hydrophilic nature make GO-MoS_2 membrane better antifouling than commercial

polymeric membranes. (Alam, Guiney et al. 2018, Alam, Guiney et al. 2019, Zhang, Gong et al. 2019)

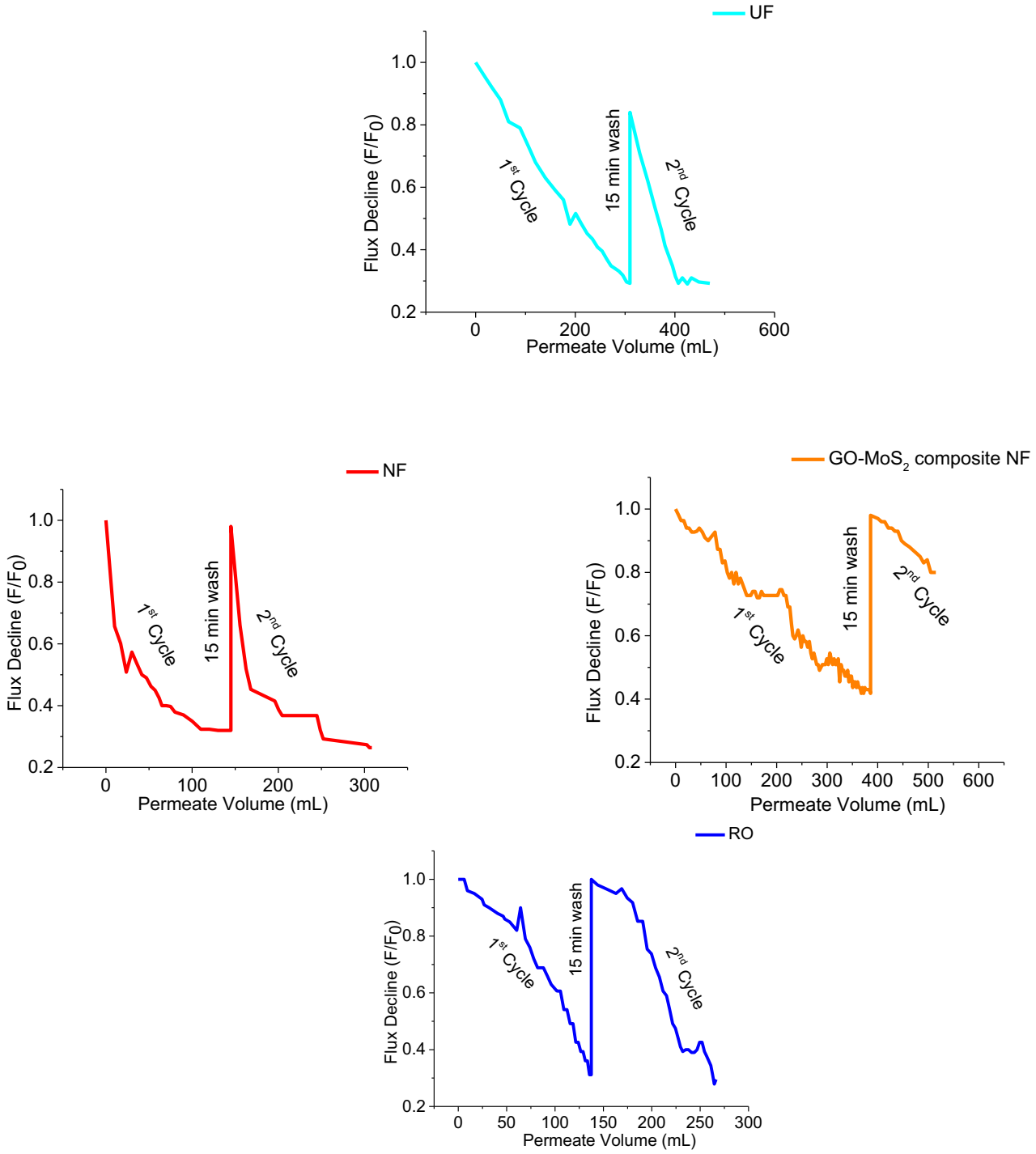

Figure 14: Normalized flux decline behavior of the membranes due to fouling

The flux recovery ratios indicate the surface regeneration capability of the membranes. Except for the UF membrane, other membranes showed excellent recovery potential with 15 min 500 mg/L NaOCl and 5 min DI water wash (Figure 15).

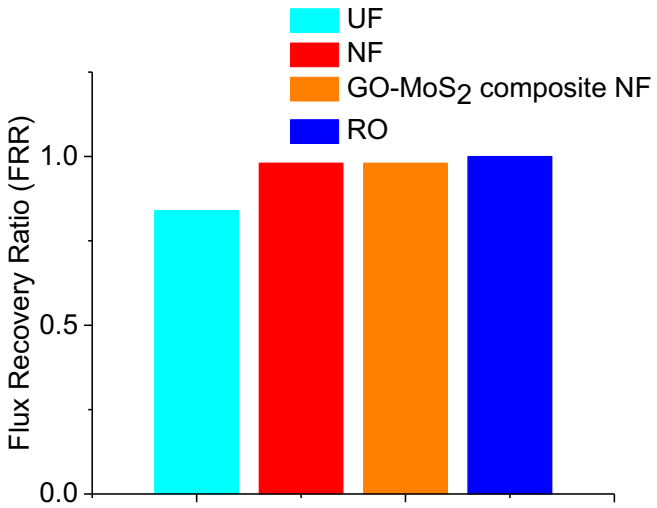

Figure 15: Normalized flux decline behavior of the membranes due to fouling

Considering the required membrane areas calculated and reported in Table 1, the total permeate volumes of the membranes were determined (Table 5). This would imply how much freshwater these membranes could provide between each wash interval. RO membrane results in the highest permeate volume but requires a lot of modules (Table 5) and higher pressure to operate.

Table 5: Permeate volume of the membranes between each wash interval

Membrane	Permeate volume (gallons) 1st cycle	Permeate volume (gallons) 2nd cycle
UF	803-7426	414-3833
NF	732-6703	540-4947
GO-MoS_2 nanocomposite NF	3247-29719	3437-29370
RO	11185-101768	10490-95452

8. CONCLUSIONS

Results show that lab prepared GO-MoS_2 NF membranes could be used for decreasing the TDS concentration of the Quincy industrial wastewater effluent to 550 mg/L, which is close to meeting EPA standard. Further modification of the composite membrane (i.e., changing the ratio of GO and MoS_2 in the mixtures, increasing the amount of nanomaterials, etc.) could result in even higher TDS removal efficiency. Though the commercial RO membrane showed a maximum 95% TDS removal efficiency, water permeability through the RO membrane was very low and it was susceptible to fast-flux decline due to fouling. On the other hand, antifouling GO-MoS_2 composite membrane treated 3 times higher wastewater effluent volume than RO membrane before each wash cycle, which will result in less frequent wash intervals and minimize the operating costs. The results of this study will be useful for designing a membrane-based treatment system in the industries for producing high-quality effluent. This would enable industrialists to reuse and recycle the polluted wastewater effluent for industrial and irrigation purposes.

ACKNOWLEDGMENTS

This work was supported by US Geological Survey grant number 11N-3815-558 via State of Washington Water Research Center**.** Sample preparation and characterization by Professor Mark C. Hersam and his group at Northwestern University were supported by the National Science Foundation and the Environmental Protection Agency under Cooperative Agreement Number DBI-1266377. We would like to thank Megan Rounds, Washington Department of Ecology for collecting the food processing wastewater samples from Quincy, WA.

REFERENCES

Akhavan, O. and E. Ghaderi (2010). ACS Nano **4**(10): 5731.

Alam, I., L. M. Guiney, M. C. Hersam and I. Chowdhury (2018). "Antifouling properties of two-dimensional molybdenum disulfide and graphene oxide." Environmental Science: Nano **5**(7): 1628-1639.

Alam, I., L. M. Guiney, M. C. Hersam and I. Chowdhury (2019). "Application of external voltage for fouling mitigation from graphene oxide, reduced graphene oxide and molybdenum disulfide functionalized surfaces." Environmental Science: Nano **6**(3): 925-936.

Alam, I., L. M. Guiney, M. C. Hersam and I. Chowdhury (2020). "Pressure-driven water transport behavior and antifouling performance of two-dimensional nanomaterial laminated membranes." Journal of Membrane Science **599**: 117812.

Angelakis, A. and S. Snyder (2015). Wastewater treatment and reuse: Past, present, and future, Multidisciplinary Digital Publishing Institute.

Arumugham, T., R. G. Amimodu, N. J. Kaleekkal and D. Rana (2019). "Nano CuO/g-C3N4 sheets-based ultrafiltration membrane with enhanced interfacial affinity, antifouling and protein separation performances for water treatment application." Journal of Environmental Sciences **82**: 57-69.

Bahnemann, D. (2004). "Photocatalytic water treatment: solar energy applications." Solar Energy **77**(5): 445-459.

Basile, A., F. Gallucci and P. Morrone (2010). 6 - Advanced carbon dioxide (CO2) gas separation membrane development for power plants. Advanced Power Plant Materials, Design and Technology. D. Roddy, Woodhead Publishing**:** 143-186.

Beyer, F., J. Laurinonyte, A. Zwijnenburg, A. J. M. Stams and C. M. Plugge (2017). "Membrane Fouling and Chemical Cleaning in Three Full-Scale Reverse Osmosis Plants Producing Demineralized Water." Journal of Engineering **2017**: 14.

Bianco Prevot, A. and E. Pramauro (1999). "Analytical monitoring of photocatalytic treatments. Degradation of 2,3,6-trichlorobenzoic acid in aqueous TiO2 dispersions1Work presented at the 5th Symposium on Analytical Sciences, Nice, France, June 1997.1." Talanta **48**(4): 847-857.

Bidsorkhi, H. C., H. Riazi, D. Emadzadeh, M. Ghanbari, T. Matsuura, W. Lau and A. Ismail (2016). "Preparation and characterization of a novel highly hydrophilic and antifouling polysulfone/nanoporous TiO2 nanocomposite membrane." Nanotechnology **27**(41): 415706.

Bouchard, D., X. Ma and C. Isaacson (2009). "Colloidal Properties of Aqueous Fullerenes: Isoelectric Points and Aggregation Kinetics of C60 and C60 Derivatives." Environmental Science & Technology **43**(17): 6597-6603.

Bouman, B. (2007). Water management in irrigated rice: coping with water scarcity, Int. Rice Res. Inst.

Campos, J. L., A. Mosquera-Corral, M. Sánchez, R. Méndez and J. M. Lema (2002). "Nitrification in saline wastewater with high ammonia concentration in an activated sludge unit." Water Research **36**(10): 2555-2560.

Cañedo-Argüelles, M., B. Kefford and R. Schäfer (2018). "Salt in freshwaters: causes, effects and prospects - introduction to the theme issue." Philosophical transactions of the Royal Society of London. Series B, Biological sciences **374**(1764): 20180002.

Chen, K. L. and M. Elimelech (2008). "Interaction of Fullerene (C60) Nanoparticles with Humic Acid and Alginate Coated Silica Surfaces: Measurements, Mechanisms, and Environmental Implications." Environ. Sci. Technol. **42**(20): 7607.

Childress, A. E. and M. Elimelech (1996). "Effect of solution chemistry on the surface charge of polymeric reverse osmosis and nanofiltration membranes." Journal of Membrane Science **119**(2): 253-268.

Chong, J. Y., B. Wang and K. Li (2018). "Water transport through graphene oxide membranes: the roles of driving forces." Chemical Communications **54**(20): 2554-2557.

Chowdhury, I., M. C. Duch, N. D. Mansukhani, M. C. Hersam and D. Bouchard (2013). "Colloidal Properties and Stability of Graphene Oxide Nanomaterials in the Aquatic Environment." Environmental Science & Technology **47**(12): 6288-6296.

Chowdhury, I., N. D. Mansukhani, L. M. Guiney, M. C. Hersam and D. Bouchard (2015). "Aggregation and Stability of Reduced Graphene Oxide: Complex Roles of Divalent Cations, pH, and Natural Organic Matter." Environmental Science & Technology **49**(18): 10886-10893.

Coskun, T., E. Debik and N. M. Demir (2010). "Treatment of olive mill wastewaters by nanofiltration and reverse osmosis membranes." Desalination **259**(1): 65-70.

de Lannoy, C.-F., D. Jassby, K. Gloe, A. D. Gordon and M. R. Wiesner (2013). "Aquatic Biofouling Prevention by Electrically Charged Nanocomposite Polymer Thin Film Membranes." Environmental Science & Technology **47**(6): 2760-2768.

Dembczynski, R. and T. Jankowski (2001). "Determination of pore diameter and molecular weight cut-off of hydrogel-membrane liquid-core capsules for immunoisolation." Journal of biomaterials science. Polymer edition **12**: 1051-1058.

Dreyer, D. R., S. Park, C. W. Bielawski and R. S. Ruoff (2010). "The chemistry of graphene oxide." Chemical Society Reviews **39**(1): 228-240.

Duch, M. C., G. R. S. Budinger, Y. T. Liang, S. Soberanes, D. Urich, S. E. Chiarella, L. A. Campochiaro, A. Gonzalez, N. S. Chandel, M. C. Hersam and G. M. Mutlu (2011). "Minimizing

Oxidation and Stable Nanoscale Dispersion Improves the Biocompatibility of Graphene in the Lung." Nano Letters **11**(12): 5201-5207.

Elimelech, M., J. Gregory, X. Jia and R. A. F. Williams (2013). Particle Deposition and Aggregation: Measurement, Modelling and Simulation, Elsevier Science.

Emadzadeh, D., W. Lau, T. Matsuura, N. Hilal and A. Ismail (2014). "The potential of thin film nanocomposite membrane in reducing organic fouling in forward osmosis process." Desalination 348: 82-88.

Erickson, H. P. (2009). "Size and shape of protein molecules at the nanometer level determined by sedimentation, gel filtration, and electron microscopy." Biological procedures online **11**(1): 32.

Esfahani, M. R., E. M. Languri and M. R. Nunna (2016). "Effect of particle size and viscosity on thermal conductivity enhancement of graphene oxide nanofluid." International Communications in Heat and Mass Transfer **76**: 308-315.

Filtration Solutions, I. from https://filtsol.com/main/index.php/technical-info/super-hydrophilic-membranes.

Geim, A.K. and Grigorieva, I.V. (2013) Nature 499(7459), 419-425.

Gao, W., L. B. Alemany, L. Ci and P. M. Ajayan (2009). "New insights into the structure and reduction of graphite oxide." Nat Chem **1**(5): 403-408.

Gebru, K. A. and C. Das (2017). "Removal of bovine serum albumin from wastewater using fouling resistant ultrafiltration membranes based on the blends of cellulose acetate, and PVP-TiO2 nanoparticles." Journal of environmental management **200**: 283-294.

Glass, C. and J. Silverstein (1999). "Denitrification of high-nitrate, high-salinity wastewater." Water Research **33**(1): 223-229.

Grant, S. B., J.-D. Saphores, D. L. Feldman, A. J. Hamilton, T. D. Fletcher, P. L. Cook, M. Stewardson, B. F. Sanders, L. A. Levin and R. F. Ambrose (2012). "Taking the “waste” out of

"wastewater" for human water security and ecosystem sustainability." science **337**(6095): 681-686.

Gu, J.-E., B.-M. Jun and Y.-N. Kwon (2012). "Effect of chlorination condition and permeability of chlorine species on the chlorination of a polyamide membrane." Water research **46**(16): 5389-5400.

Han, B., T. Runnells, J. Zimbron and R. Wickramasinghe (2002). "Arsenic removal from drinking water by flocculation and microfiltration." Desalination **145**(1): 293-298.

Hartono, T., S. Wang, Q. Ma and Z. Zhu (2009). "Layer structured graphite oxide as a novel adsorbent for humic acid removal from aqueous solution." Journal of Colloid and Interface Science **333**(1): 114-119.

Heiranian, M., A. B. Farimani and N. R. Aluru (2015). "Water desalination with a single-layer MoS2 nanopore." Nat Commun **6**.

Heiranian, M., A. B. Farimani and N. R. Aluru (2015). "Water desalination with a single-layer MoS(2) nanopore." Nature Communications **6**: 8616.

Hilal, N., H. Al-Zoubi, N. A. Darwish, A. W. Mohamma and M. Abu Arabi (2004). "A comprehensive review of nanofiltration membranes:Treatment, pretreatment, modelling, and atomic force microscopy." Desalination **170**(3): 281-308.

Hoek, E. M., M. T. M. Pendergast and A. K. Ghosh (2014). Nanotechnology-based membranes for water purification. Nanotechnology applications for clean water, Elsevier**:** 133-154.

Hou, W.-C., I. Chowdhury, D. G. Goodwin, W. M. Henderson, D. H. Fairbrother, D. Bouchard and R. G. Zepp (2015). "Photochemical Transformation of Graphene Oxide in Sunlight." Environmental Science & Technology **49**(6): 3435-3443.

Hu, M. and Mi, B. (2014) Journal of Membrane Science 469, 80-87.

Huang, H., Z. Song, N. Wei, L. Shi, Y. Mao, Y. Ying, L. Sun, Z. Xu and X. Peng (2013). "Ultrafast viscous water flow through nanostrand-channelled graphene oxide membranes." Nature Communications **4**(1): 2979.

Jiraratananon, R., A. Sungpet and P. Luangsowan (2000). "Performance evaluation of nanofiltration membranes for treatment of effluents containing reactive dye and salt." Desalination **130**(2): 177-183.

Karagiannis, I. C. and P. G. Soldatos (2008). "Water desalination cost literature: review and assessment." Desalination **223**(1): 448-456.

Kim, S., D. Dehlinger, J. Peña, H. Seol, M. Shusteff, N. M. Collette, M. Elsheikh, M. Davenport, P. Naraghi-Arani and E. Wheeler (2019). "Virus concentration and purification by a microfluidic filtering system with an integrated PEGylated antifouling membrane." Microfluidics and Nanofluidics **23**(1): 9.

Landschoot, P. (2014). Irrigation water quality guidelines for turfgrass sites.

Lanphere, J. D., C. J. Luth, L. M. Guiney, N. D. Mansukhani, M. C. Hersam and S. L. Walker (2015). "Fate and Transport of Molybdenum Disulfide Nanomaterials in Sand Columns." Environmental Engineering Science **32**(2): 163-173.

Lau, W.-J. and A. F. Ismail (2009). "Polymeric nanofiltration membranes for textile dye wastewater treatment: Preparation, performance evaluation, transport modelling, and fouling control — a review." Desalination **245**(1): 321-348.

Li, M.-N., X.-F. Sun, L. Wang, S.-Y. Wang, M. Z. Afzal, C. Song and S.-G. Wang (2018). "Forward osmosis membranes modified with laminar MoS 2 nanosheet to improve desalination performance and antifouling properties." Desalination **436**: 107-113.

Li, Q. and M. Elimelech (2004). "Organic Fouling and Chemical Cleaning of Nanofiltration Membranes: Measurements and Mechanisms." Environmental Science & Technology **38**(17): 4683-4693.

Lin, J. and S. Murad (2001). "A computer simulation study of the separation of aqueous solutions using thin zeolite membranes." Molecular Physics **99**(14): 1175-1181.

Lin, Z., C. Hu, X. Wu, W. Zhong, M. Chen, Q. Zhang, A. Zhu and Q. Liu (2018). "Towards improved antifouling ability and separation performance of polyethersulfone ultrafiltration membranes through poly (ethylenimine) grafting." Journal of membrane science **554**: 125-133.

Liu, Y. and B. Mi (2012). "Combined fouling of forward osmosis membranes: Synergistic foulant interaction and direct observation of fouling layer formation." Journal of membrane science **407**: 136-144.

Lohwacharin, J., K. Oguma and S. Takizawa (2009). "Ultrafiltration of natural organic matter and black carbon: Factors influencing aggregation and membrane fouling." Water research **43**(12): 3076-3085.

Madaeni, S. S., E. Rostami and A. Rahimpour (2010). "Surfactant cleaning of ultrafiltration membranes fouled by whey." International journal of dairy technology **63**(2): 273-283.

Mays, L. W. (2007). Water resources sustainability, McGraw-Hill New York.

Mi, B. and M. Elimelech (2010). "Organic fouling of forward osmosis membranes: fouling reversibility and cleaning without chemical reagents." Journal of membrane science **348**(1-2): 337-345.

Muhammad, Y. and W. Lee (2019). "Zero-liquid discharge (ZLD) technology for resource recovery from wastewater: A review." Science of The Total Environment **681**: 551-563.

Mukherjee, R., P. Bhunia and S. De (2016). "Impact of graphene oxide on removal of heavy metals using mixed matrix membrane." Chemical Engineering Journal **292**: 284-297.

Nguyen, T., F. A. Roddick and L. Fan (2012). "Biofouling of Water Treatment Membranes: A Review of the Underlying Causes, Monitoring Techniques and Control Measures." Membranes **2**(4): 804-840.

Oren, Y., E. Korngold, N. Daltrophe, R. Messalem, Y. Volkman, L. Aronov, M. Weismann, N. Bouriakov, P. Glueckstern and J. Gilron (2010). "Pilot studies on high recovery BWRO-EDR for near zero liquid discharge approach." Desalination **261**(3): 321-330.

Otaki, M., K. Yano and S. Ohgaki (1998). "Virus removal in a membrane separation process." Water Science and Technology **37**(10): 107-116.

Pendergast, M. M. and E. M. V. Hoek (2011). "A review of water treatment membrane nanotechnologies." Energy & Environmental Science **4**(6): 1946-1971.

Perreault, F., M. E. Tousley and M. Elimelech (2014). "Thin-Film Composite Polyamide Membranes Functionalized with Biocidal Graphene Oxide Nanosheets." Environmental Science & Technology Letters **1**(1): 71-76.

Pramauro, E., A. B. Prevot, M. Vincenti and R. Gamberini (1998). "Photocatalytic degradation of naphthalene in aqueous TiO2 dispersions: Effect of nonionic surfactants." Chemosphere **36**(7): 1523-1542.

Ray, J. R., S. Tadepalli, S. Z. Nergiz, K.-K. Liu, L. You, Y. Tang, S. Singamaneni and Y.-S. Jun (2015). "Hydrophilic, Bactericidal Nanoheater-Enabled Reverse Osmosis Membranes to Improve Fouling Resistance." ACS Applied Materials & Interfaces **7**(21): 11117-11126.

Ruiz-García, A., N. Melián-Martel and I. Nuez (2017). "A Critical Review on Predicting Fouling in RO Desalination."

Sagle, A. and B. Freeman (2004). "Fundamentals of membranes for water treatment." The future of desalination in Texas **2**(363): 137.

Sato T, Qadir M, Yamamoto S, Endo T, Zahoor A, Agricultural Water Management, 2013, 130, 1.

Seidel, A. and M. Elimelech (2002). "Coupling between chemical and physical interactions in natural organic matter (NOM) fouling of nanofiltration membranes: implications for fouling control." Journal of Membrane Science **203**(1): 245-255.

Shin, D. H., N. Kim and Y. T. Lee (2011). "Modification to the polyamide TFC RO membranes for improvement of chlorine-resistance." Journal of membrane science **376**(1-2): 302-311.

Sobsey, M. D., C. E. Stauber, L. M. Casanova, J. M. Brown and M. A. Elliott (2008). "Point of Use Household Drinking Water Filtration: A Practical, Effective Solution for Providing Sustained Access to Safe Drinking Water in the Developing World." Environmental Science & Technology **42**(12): 4261-4267.

Sri Abirami Saraswathi, M. S., D. Rana, P. Vijayakumar, S. Alwarappan and A. Nagendran (2017). "Tailored PVDF nanocomposite membranes using exfoliated MoS2 nanosheets for improved permeation and antifouling performance." New Journal of Chemistry **41**(23): 14315-14324.

Sun, L., H. Huang and X. Peng (2013). "Laminar MoS 2 membranes for molecule separation." Chemical communications **49**(91): 10718-10720.

Systems, P. C. I. W. from https://www.purichem-eg.com/services-item/desalination-plants/.

Tong, T. and M. Elimelech (2016). "The Global Rise of Zero Liquid Discharge for Wastewater Management: Drivers, Technologies, and Future Directions." Environmental Science & Technology **50**(13): 6846-6855.

Tsuneda, S., M. Mikami, Y. Kimochi and A. Hirata (2005). "Effect of salinity on nitrous oxide emission in the biological nitrogen removal process for industrial wastewater." Journal of Hazardous Materials **119**(1): 93-98.

Ulbricht, M. (2006). "Advanced functional polymer membranes." Polymer **47**(7): 2217-2262.

Vatanpour, V., S. S. Madaeni, R. Moradian, S. Zinadini and B. Astinchap (2012). "Novel antibifouling nanofiltration polyethersulfone membrane fabricated from embedding TiO2 coated multiwalled carbon nanotubes." Separation and Purification Technology **90**: 69-82.

Vrijenhoek, E. M. and J. J. Waypa (2000). "Arsenic removal from drinking water by a "loose" nanofiltration membrane." Desalination **130**(3): 265-277.

Wang, J., P. Zhang, B. Liang, Y. Liu, T. Xu, L. Wang, B. Cao and K. Pan (2016). "Graphene Oxide as an Effective Barrier on a Porous Nanofibrous Membrane for Water Treatment." ACS Applied Materials & Interfaces **8**(9): 6211-6218.

Wang, Q. H., K. Kalantar-Zadeh, A. Kis, J. N. Coleman and M. S. Strano (2012). "Electronics and optoelectronics of two-dimensional transition metal dichalcogenides." Nat Nano **7**(11): 699-712.

Wang, W., L. Zhu, B. Shan, C. Xie, C. Liu, F. Cui and G. Li (2018). "Preparation and characterization of SLS-CNT/PES ultrafiltration membrane with antifouling and antibacterial properties." Journal of Membrane Science **548**: 459-469.

Wang, Z. and B. Mi (2017). "Environmental Applications of 2D Molybdenum Disulfide (MoS2) Nanosheets." Environmental Science & Technology **51**(15): 8229-8244.

Wang, Z., Q. Tu, S. Zheng, J. J. Urban, S. Li and B. Mi (2017). "Understanding the Aqueous Stability and Filtration Capability of MoS2 Membranes." Nano letters **17**(12): 7289-7298.

Wei, N., X. Peng and Z. Xu (2014). "Understanding water permeation in graphene oxide membranes." ACS applied materials & interfaces **6**(8): 5877-5883.

Wu, G., S. Gan, L. Cui and Y. Xu (2008). "Preparation and characterization of PES/TiO2 composite membranes." Applied Surface Science **254**(21): 7080-7086.

WWAP (2019). The United Nations World Water Development Report 2019: Leaving No One Behind, UNESCO Paris.

Zhang, H. (2015). "Ultrathin Two-Dimensional Nanomaterials." ACS Nano **9**(10): 9451-9469.

Zhang, P., J.-L. Gong, G.-M. Zeng, B. Song, W. Cao, H.-Y. Liu, S.-Y. Huan and P. Peng (2019). "Novel “loose” GO/MoS2 composites membranes with enhanced permeability for effective salts and dyes rejection at low pressure." Journal of Membrane Science **574**: 112-123.

Zheng, S., Q. Tu, J. J. Urban, S. Li and B. Mi (2017). "Swelling of graphene oxide membranes in aqueous solution: characterization of interlayer spacing and insight into water transport mechanisms." ACS nano **11**(6): 6440-6450.

Zhu, J., M. Tian, J. Hou, J. Wang, J. Lin, Y. Zhang, J. Liu and B. Van der Bruggen (2016). "Surface zwitterionic functionalized graphene oxide for a novel loose nanofiltration membrane." Journal of Materials Chemistry A **4**(5): 1980-1990.

Zodrow, K. R., E. Bar-Zeev, M. J. Giannetto and M. Elimelech (2014). "Biofouling and Microbial Communities in Membrane Distillation and Reverse Osmosis." Environmental Science & Technology **48**(22): 13155-13164.

APPENDIX

US Geological Survey: 11N-3815-558

Project Title: Reuse of Food Processing Wastewater in Washington State

PI: Indranil Chowdhury

Co-PI: Lynne Carpenter-Boggs

Student Support		
Degree Level	Number of Students	Number of Dissertations/Theses Resulting from Student Support
Undergraduate	0	0
Masters	0	0
Ph.D.	1	1
Post Doctoral	0	0

Students name, Degree Level

Iftaykhairul Alam, Ph.D.

Publications	
Publication Type	**Publication Citation**
Journal	Alam, I., Guiney, L.M., Hersam, M.C., **Chowdhury, I.** (2020) "Pressure-driven Filtration and Antifouling Performance of Two-Dimensional Nanomaterial Functionalized Membranes", Journal of Membrane Science, 599, 117812.
Conference	Alam, I., Guiney, L.M., Hersam, M.C., **Chowdhury, I.** "Novel Graphene Oxide and Molydenum Disulfide Composite Membranes with Improved Desalination and Antifouling Performance", presented at Sustainable Nanotechnology Conference, November 11-13, 2020.
Invited Seminar	**Chowdhury, I.,** "Two Dimensional Nanomaterial-based Membranes for Water Filtration", webinar presented at USAID Center of Excellence for Water, September 1, 2020.
Conference	Alam, I., **Chowdhury, I. "**Reuse of Food Processing Wastewater in Irrigation using Two-Dimensional Nanomaterial-Based Membranes", presented at ACS Fall 2020 Virtual Meeting & Expo, August 17-20, 2020.
Conference	Alam, I., Guiney, L.M., Hersam, M.C., **Chowdhury, I. "**Pressure-driven Filtration and Antifouling Performance of Two Dimensional Nanomaterial Functionalized Membranes", presented at 8th Sustainable Nanotechnology Conference, November 7-9, 2019, San Diego, CA.

Follow On	
Source and Amount of Funding	**Funding Period**
USDA NIFA; $499,753 (Title: Reuse of Treated Food Processing Wastewaters in Irrigation) (Co-PI: Lynne Carpenter-Boggs)	Applied (2021-2024)